N83-25039

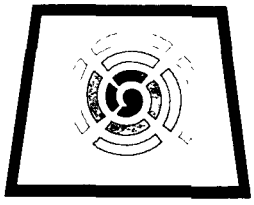

THE UNIVERSITY OF NEW MEXICO
COLLEGE OF ENGINEERING

BUREAU OF ENGINEERING RESEARCH

STUDY OF THE PHOTOVOLTAIC EFFECT IN THIN FILM BARIUM TITANATE

BY

W. W. GRANNEMANN
AND
VINEET S. DHARMADHIKARI

REPORT NO. EECE-275(83)NASA-931-1

WORK PERFORMED UNDER CONTRACT NO. NAG-1-95

FEBRUARY 1983

Final Report

on

STUDY OF THE PHOTOVOLTAIC EFFECT IN THIN FILM BARIUM TITANATE

by

W. W. Grannemann
and
Vineet S. Dharmadhikari

Department of Electrical and Computer Engineering
The University of New Mexico
Albuquerque, New Mexico 87131

Report No. EECE-275(83)NASA-931-1
Work Performed Under Contract No. NAG-1-95

February 1983

TABLE OF CONTENTS

LIST OF FIGURES

LIST OF FIGURES (Continued)

INTRODUCTION

Our work on barium titanate, $BaTiO_3$, examined the feasibility of making non-volatile digital memory devices, that are integrated onto a silicon substrate with the required ferroelectric film produced by processing, compatible with silicon technology.

Barium titanate was chosen as the starting material primarily for two reasons: the ferroelectric properties of the material have been well characterized, and its simple structure makes it an ideal choice for such studies. Moreover, we have successfully rf sputter-deposited $BaTiO_3$ thin films in MFIS capacitor applications [2, 3]. In addition, because of the high dielectric constant of the ferroelectric films, the transconductance and amplification gain are higher; consequently memory devices fabricated with a ferroelectric layer as a dielectric have a number of advantages over other memory devices. Furthermore, the absence of any kind of photovoltaic study in the current literature also enhances the importance of such an investigation.

Single-crystal silicon substrates were selected instead of fused quartz, platinum or sodium fluoride. Generally, previous investigators have preferred these substrates because of the silicon's virtual monopoly in the fabrication of integrated circuits in the microelectronics industry. Of the various methods available in growing thin films, rf sputtering was chosen because it offers greatest control over the nature of the resulting films. Compared to physical evaporation techniques, sputtering is lower in cost, more reproducible, and provides more uniformly thick layers over larger areas.

Our program performed the intensive studies necessary for NASA's initial step in synthesizing ferroelectric thin films of $BaTiO_3$ on single-crystal silicon substrates using rf sputtering technique as well as studying their photovoltaic properties. In addition, the study also provides important information on the basic mechanism associated with the observed photovoltaic phenomena and the thin-film technology of sputtered $BaTiO_3$/silicon system.

A high-voltage photovoltaic effect in poled ferroelectric ceramic materials is a relatively recent discovery [1]. The steady photo-emfs generated in these ferroelectric ceramics are proportional to remanent polarization. Also the polarity of these photo-emfs depends on the direction of the remanent polarization. These typically 1000 v/cm photo-emf's are considered in excess of band gap potential difference; hence the term anomalous photovoltaic effect is used to describe them.

The remainder of this report has seven major sections: Experimental Details, Theory, Results and Discussion, Photovoltaic Effect, Auger Analysis, Effects of Surface Layers on Ferroelectric Properties, and Summaries and Conclusions. The first section discusses the instrumentation used to fabricate the devices and characterizes the MFS structures, while the following section documents the theory dealing with the ferroelectrics and the photoferroelectric effects observed. In the next section, the observed experimental results are presented and discussed. These results show that ferroelectric behavior is regularly observed for tetragonal $BaTiO_3$ films thicker than 1000 Å that are rf-sputter deposited at 5 Å/min in 18 to 22 μm Hg pressure, 5% O_2/95% Ar mixture onto silicon substrate initially above 500°C. The results on open circuit photovoltage and short circuit photocurrents also provide an important basis for a better understanding of the role of photovoltaic field and photovoltaic current in

photoferroelectric domain switching. The results reported in this section as well as in the following section, Photovoltaic Effect, indicate an interaction between the deposited film and the substrate which poisons the film. This finding led us to investigate the chemical composition and the $BaTiO_3$/Si interface. These results are presented in the section entitled Auger Analysis. The effect of these surface layers on the ferroelectric properties is discussed in the next section which also discusses the promising, although very preliminary, qualitative interpretation of the data. The first section summarizes the present work and provides references. Two papers were published based on work supported or inititated by this program; these papers are reproduced in Appendix 1.

EXPERIMENTAL DETAILS

In this section the use of rf sputtering deposition technique for the growth of thin ferroelectric films of $BaTiO_3$ on single-crystal silicon substrates is discussed. The other structural and electrical measurements used to characterize the MFS structures are also presented.

Sample Preparation

Thin films of $BaTiO_3$ were sputtered using a highly modified rf diode sputtering system (CVC Model AST 300) with a lower driven electrode holding a 5-inch diameter 99.99% pure $BaTiO_3$ target. Sputtering occurred upwards onto a 7-inch diameter grounded electrode holding a 2 1/2-inch square substrate heater, mask, and substrate at the center (Figure 1). A shutter with a magnetic feed-through was installed in-between the driven electrode and the $BaTiO_3$ target. Except where noted, all metal parts in the vacuum chamber were fabricated from non-magnetic stainless steel or were copper plated with high purity nickel. A Keithley

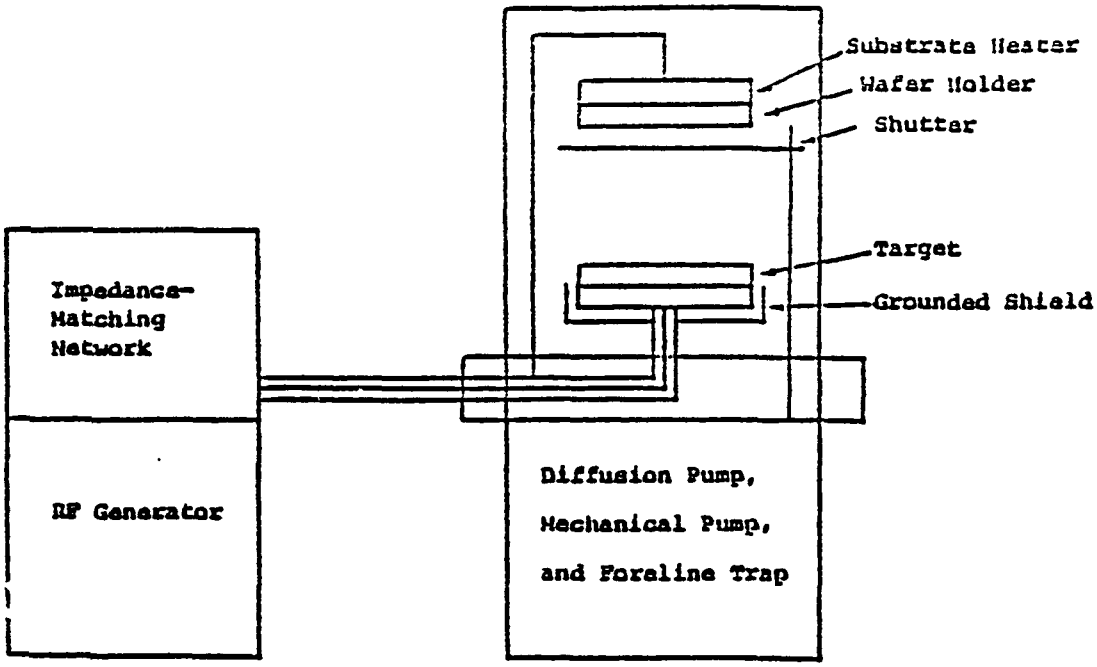

Figure 1. Schematic diagram of sputtering and vacuum system.

600A electrometer with a 1000:1 voltage divider measured the inherent bias developed on the target electrode, with respect to the positive ions. This parameter is more meaningful than "power input" to an rf sputtering system since some of the input is dissipated in the walls of the vacuum chamber and fixtures. Slow deposition (5 to 10 Å/min) corresponding to a target bias of -400 to 550 V at various substrate temperatures (55 to 750°C) were investigated.

A standard high-vacuum pumping system was employed. The system consisted of a 6-inch diameter oil diffusion pump with a freon trap and a rotary vane foreline pump with a molecula sieve trap. The ultimate system pressure was about 4×10^{-8} torr. Before the sputtering session, ultrahigh purity oxygen and argon were bled into the system for a typical 5 to 10% O_2 in an argon-oxygen mixture. After the desired percent mixture had been obtained, the high-vacuum valve was choked down to get the desired sputtering pressure in the bell jar; this was in the 18 to 22 μm range. During every sputtering session, the $BaTiO_3$ target was sputtered clean at least for one hour before opening the shutter to deposit onto the silicon substrate. A few samples after the deposition were heat treated at 800 to 1000°C in different ambients, namely: Ar, O_2, N_2, and O_2/N_2 mixtures for time varying between 5 minutes to 4 hours.

A special substrate heater capable of maintaining temperatures up to 800°C during an 8-hour experiment was used [3] (Figure 2). It consists of two 1 1/3 Ω resistance strips of nickel-chromium alloy ribbon folded in a serpentine pattern and connected in parallel to a 40 A 40 Vdc power supply. A sandwich consisting of a 0.7-mm-thick piece of alumina (for electrical isolation), a 1.5-mm-thick piece of nickel-plated copper (for even heat distribution), and a 1.5-mm-thick sapphire plate was

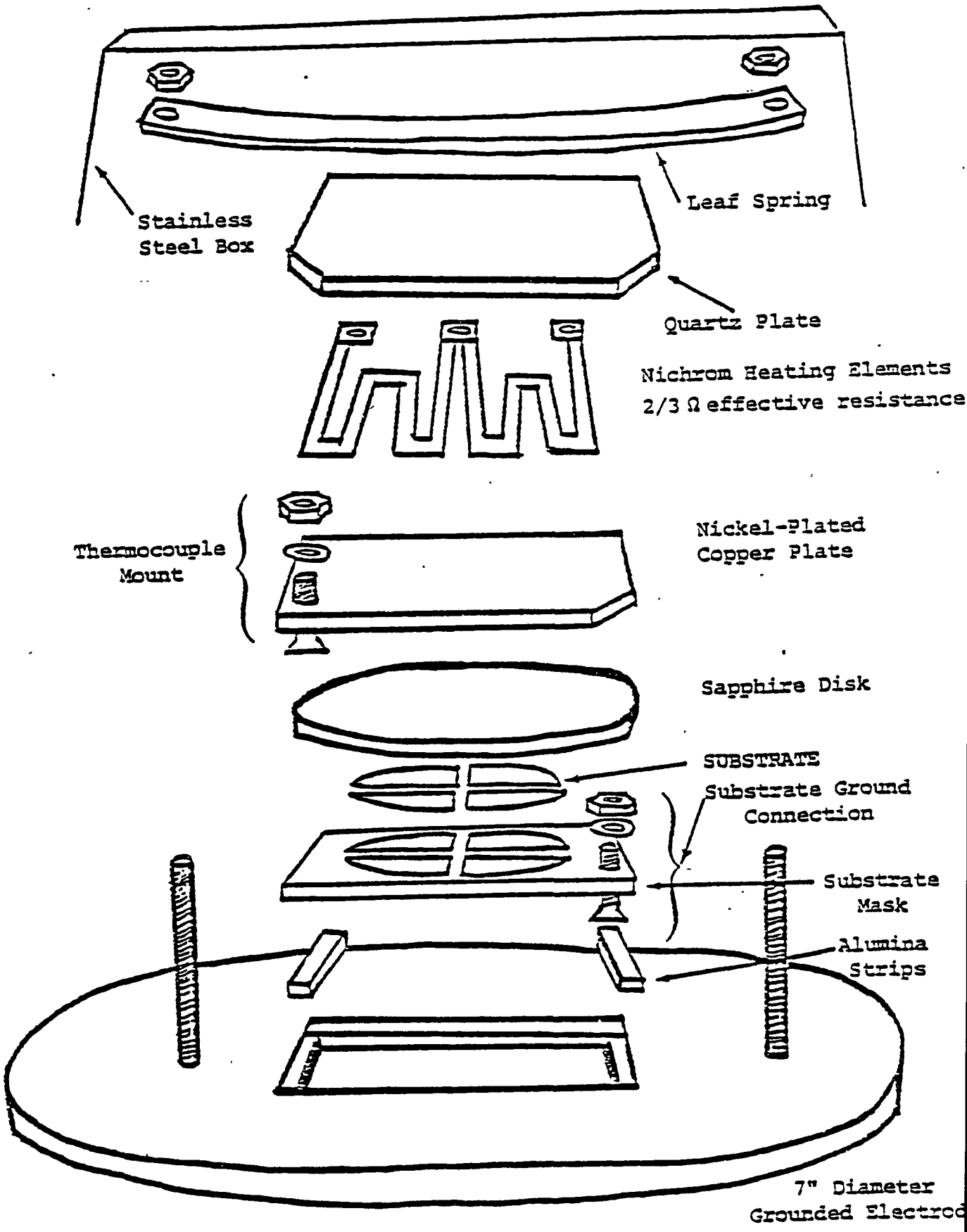

Figure 2. Substrate heater assembly (~2-1/2" x 2-1/2").

placed in-between the heater and the back surface of silicon substrate. The sapphire plate was added to avoid the interaction of the back surface of silicon with the nickel-plated copper plate, especially for deposition done at higher substrate temperatures. A quartz plate, a tantalum foil heat reflector, and another quartz plate and tantalum foil were placed on the heating elements for higher temperature runs. Good thermal contact between the various layers of the heating unit was assured by spring loading the entire assembly. A heat reflector fabricated of 0.7 mm stainless steel sheet metal surrounded the heater. A chromel-alumel thermocouple held tightly by a nut and bolt in contact with the nickel-plated copper plate measured the substrate temperature. In practice, temperature measurements were taken before opening the shutter, after preheating the substrate, and one hour before the conclusion of the run. The time substrate temperature was within the ±50°C limit for the higher deposition temperatures.

Single-crystal silicon wafers doped with phosphorus (n-type) and cleaved parallel to the (100) plane were used as substrate material. The resistivity was 5 Ω-cm which corresponds to a 1×10^5 atoms/cm^3 doping level. Before film deposition, the wafers were thoroughly cleaned and etched in an Hf buffer solution to strip off the SiO_2 layer. After cleaning, the substrates were blown dry by pre-purified nitrogen. The wafers were then mounted on the substrate heater assembly, and the assembly was mounted in the vacuum system which was pumped down to the 10^8 torr range. To test the ferroelectric properties of the $BaTiO_3$ films, a metal-insulator-semiconductor (MIS) structure was formed. Silicon wafers were used as the lower electrode and a layer of high purity (99.99%) gold was thermally evaporated on the back of each wafer. Then the wafers were heat treated to

400°C for 5 minutes to ensure eutectic bonding between the silicon and gold. This procedure gave a good ohmic contact between the probe and the wafer. The upper electrode was generally formed by thermal evaporation of high-purity (99.99%) chromium pellets; however, in a few cases, indium tin oxide (ITO) was used as the upper electrode.

The gold and chromium evaporations were performed from resistively heated tungsten wire elements at pressures in the range of 10^{-6} torr. The procedure took place in a standard vacuum system pumped by a 4-inch diameter straight-stack oil diffusion pump with a liquid nitrogen trap and a rotary vane roughing pump. A shutter isolated the substrate from the evaporator at the beginning of the thermal evaporation process.

Electrical Measurements

Capacitance was measured as a function of voltage at 1 MHz characteristic frequency of a Boonton Model 71A capacitance meter. By superimposing a slowly varying (5 to 10 cycles/min) sine wave with an amplitude of 20 V onto the 1 MHz frequency, a continuous C-V curve was generated. The temperature of the sample was monitored by a Chromel-Alumel thermocouple attached to the sample. Polarization as a function of electric field was also measured at different frequencies (6, 60, 600 and 6 kHz) with a conventional Sawyer-Tower circuit, and a Tectronix Model 454 oscilloscope was used to display the output.

The open circuit photovoltage and short-circuit photocurrents were measured using a Victoreen electrometer (Model 475B) with an input impedance of greater than 10^{12} Ω. Illumination was from a high-intensity monochromatic ultraviolet source of 366 nm, roughly that of the band-gap energy. Intensity was calibrated with the help of a Blakray ultraviolet intensity meter placed in the path of the light flux with the device removed. The photovoltage and photocurrent measurements were made at thermal equilibrium.

Structure and Chemical Composition

The structure of the target material and the sputtered films was analyzed by x-ray diffraction technique using $CuK_{\alpha 1}$ radiation. The surface structure of the films was examined by a scanning electron microscope attached to an EDX system.

The composition depth profiles of the sputtered films were obtained with the help of a Physical Electronics Industries (PHI) Model 590 Scanning Auger system. The vacuum system was degassed until a base pressure of about 10^{-10} torr was reached. The primary beam energy ep was 50 keV permitting the beam size to be reduced to 0.2 μm by electrostatic focusing. The AES data were recorded in the usual first derivative mode $\frac{dnCE}{dE}$ using 4V peak-to-peak modulation and 1m sec time constant (RC). The depth profiles were recorded by sputtering with 8 kV Ar^+ ions and ion gun emission current up to 25 mA was used.

THEORY

In this section the general theory associated with the ferroelectric and the photoferroelectric effects observed in materials is described.

Ferroelectricity

A crystal is called ferroelectric when it has two or more orientational states in the absence of an electric field and can be shifted from one to another of these states by an electric field. Any two of these orientation states are identical (or enantiomorphous) in crystal structure and differ only in electric polarization vector at null electric field. Typically, some threshold coercive electric field is necessary to switch the polarization vector from a maximum in one direction to a maximum in the opposite direction. A ferroelectric crystal will retain

some remanent polarization after the coercive field is removed and there is no applied field. It follows that the relationship between the polarization $\vec{P}$, and the applied electric field $\vec{E}$ (or, equivalently, the capacitance, C, and the applied voltage, V) for a ferroelectric material is a hysteresis curve.

Since the alignment of the electric dipoles always switches to increase the polarization of the crystal in the direction of the applied field, the sense of the hysteresis curve associated with ferroelectric behavior is counterclockwise. For a MIS system involving two different insulators, such as $BaTiO_3$ on a layer of SiO_2 on silicon, the free carriers in the silicon may tunnel through the SiO_2 to become trapped at the SiO_2-$BaTiO_3$ boundary layer when the applied electric field reaches a certain threshold value. For some threshold value of the electric field in the opposite direction, the free charge will tunnel back into the silicon. This tunneling phenomenon results in a hysteresis curve, $\vec{P}$ vs $\vec{E}$ relationship with a clockwise sense since the free charge always tunnels in a direction to reduce the polarization of the system. When working with a ferroelectric dielectric system, such as the case of the present study, it is necessary to observe the sense of the hysteresis curves.

The first ferroelectric perovskite to be discovered was $BaTiO_3$. Since then it has been one of the most intensively studied ferroelectrics [4]. Bulk single crystal $BaTiO_3$ has the prototype cubic perovskite structure (point group m3m) with a lattice constant of 4.01 Å above 120°C. Below 120°C it transforms successively to three ferroelectric phases: first to 4 mm tetragonal, then to mm orthorhombic at about 5°C, and finally to a 2m trigonal phase below -90°C. The polar axis in the three ferroelectric phases is [001], [011], and [111] respectively. The room temperature phase (i.e., the 4 mm tetragonal) has lattice constants a = 4.00Å and c = 4.04 Å, a coercive field value

between 500 and 2000 v/cm, a remanent polarization of 26 x 10^{-6} coulomb/cm^2, and a dielectric constant at 60 Hz equal to 200 in the c direction and 400 in the a direction. The refractive index of bulk single crystal $BaTiO_3$ at room temperature is 24.

The parallel alignment of dipoles in a ferroelectric is due primarily to a relatively strong long range interaction (L_c) along the polar c-axis and a weaker shorter range (L_a) interaction normal to the axis. Although the quantitative manner in which the correlation lengths L_a and L_c as defined by different workers may vary a little, typical values for many ferroelectrics are L_c ~100-500Å and L_a = 10-20 Å. These values show that the transverse correlation range L_a is of the same order as the thickness of a 180° domain wall while the polar axis range L_c can amount to many tens of unit-cell lengths. Consequently, as the physical dimensions of the crystal are reduced, a change in the stability of the ferroelectric phase is to be expected. Therefore, the physical parameters of a thin film can be quite different from those values for bulk material. In reality the perturbing effects of defects structure in films (the surface tension and surface dipole layers) may make important contributions to the characteristics of a thin film. In practice, in trying to deposit ferroelectric thin films of $BaTiO_3$,one must first obtain thin films 1) that have the same stoichiometry as the bulk, 2) that exhibit long range (greater than 100 to 200 Å) [5-7] crystalline order, 3) that have tetragonal structure at room temperature, and 4) that have a stable equilibrium state for which the titanium ion is displaced from the center of the oxygen ions. This displacement results in a dipole moment.

Photoferroelectric Effect

Conventional photovoltaic effects fall into two general classes. The first class arises from the Dember effect where the photovoltage develops between the front and back surfaces of a

crystal when the front face is illuminated with light energy greater than the electronic band gap. The light is absorbed as it penetrates the crystal resulting in a gradient of the free carrier concentrations (both electrons and holes) through the crystal thickness. The voltage results from a difference in mobilities of electrons and holes created at the illuminated surface. The second class arises with homogenous absorption in crystals containing macroscopic inhomogeneitiess. These cause band bending such as p-n functions. Excess photocarriers diffuse in opposite directions under the influence of space-charge fields. In all of these cases the magnitude of the photovoltage across a single element cannot exceed the value of the electronic energy gap. In pyroelectric materials, the spontaneous polarization gives rise to new photovoltaic effects which are not observed in materials with a center of symmetry and which are not necessariy limited to voltages less than the band gap. Thus, the special feature that characterizes a pyroelectric is the existence of polar axis in the crystal lattice. The ferroelectrics are a subclass of the pyroelectrics; all ferroelectrics exhibit pyroelectricity, but a pyroelectric need not be ferroelectric.

Current Theories

Two theories [1, 8] are currently used to interpret the anomalously large photovoltage obtained under open-circuit conditions in a number of pyroelectrics more in qualitative than in quantitative terms.

Brody's model [1] has been used mostly in an attempt to explain the large photovoltages seen in polarized samples of ceramic ferroelectrics. According to his model, in the absence of illumination the ferroelectric polarization charges within each ceramic grain are presumed to be neutralized by compensation charges. When the ceramic is illuminated, photogenerated carriers neutralize the polarization charges thereby exposing the

compensation charges which can then act to produce an electric field in the grain. The integral of field across the grain gives rise to an elemental photovoltage. When the ceramic is poled, the spontaneous polarization of the collective system of grains tends to align along the poling axis and the elemental photovoltages, similarly aligned, add from grain to grain.

Figure 3 shows a planar model of a representative grain. It is assumed that the spontaneous polarization P_o falls continuously to zero at the planes $x = \delta$ and $L - \delta$, and the resultant divergence in polarization gives rise to surface charge densities $-P_o$ and $+P_o$ at the respective surfaces. In the dark, these charges are partially neutralized by compensation charges that are developed in a thickness of $\delta << L$. Inside the bulk of the grain $\delta < x < L - \delta$, a negatively directed E field exists. When the grain is illuminated, the electron-hole pairs generated within the grain's bulk move under the influence of the residual E-field to the ends of the grain, and by doing so, cancel the E-field in the bulk. The photovoltage per grain is then obtained by integrating this field from $x = L$ to 0 and is given by

$$V = \frac{\alpha P_o \delta}{\varepsilon} \qquad (1)$$

The point $x = 0$ is the positive end of the grain and therefore, the sign of the photovoltage has the same polarity as the voltage used to establish the spontaneous polarization.

In the Glass et al. model [8] the photoeffect is attributed to the photoexcitation of electrons trapped in anisotropic potential wells. The mechanism is illustrated in Figure 4. In the dark, the trapped electron is in the ground state E_o of an anisotropic potential well. When light of sufficient energy is applied, the electron is raised from ground state to a state of

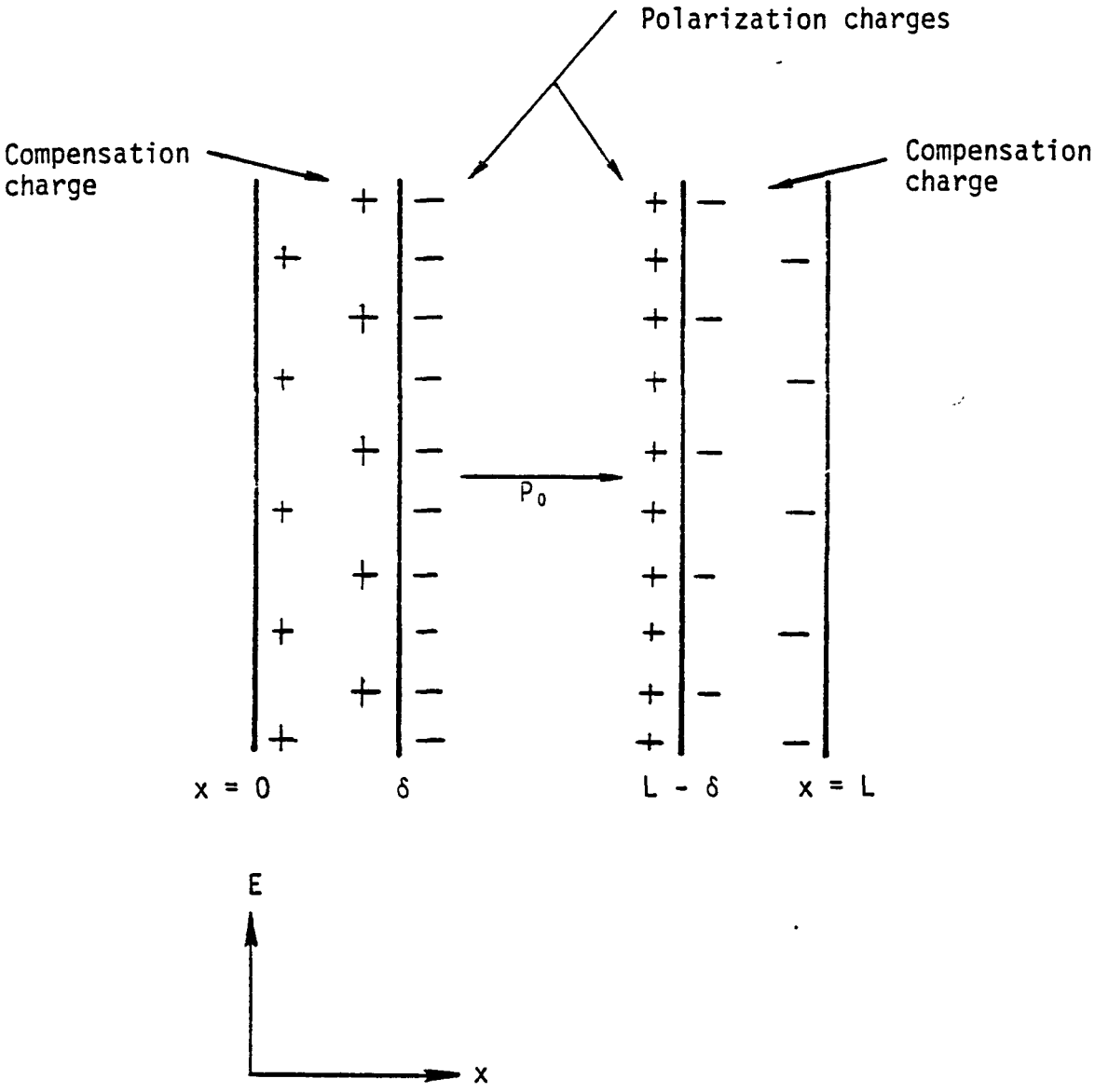

Figure 3. Model for ferroelectric "grain".

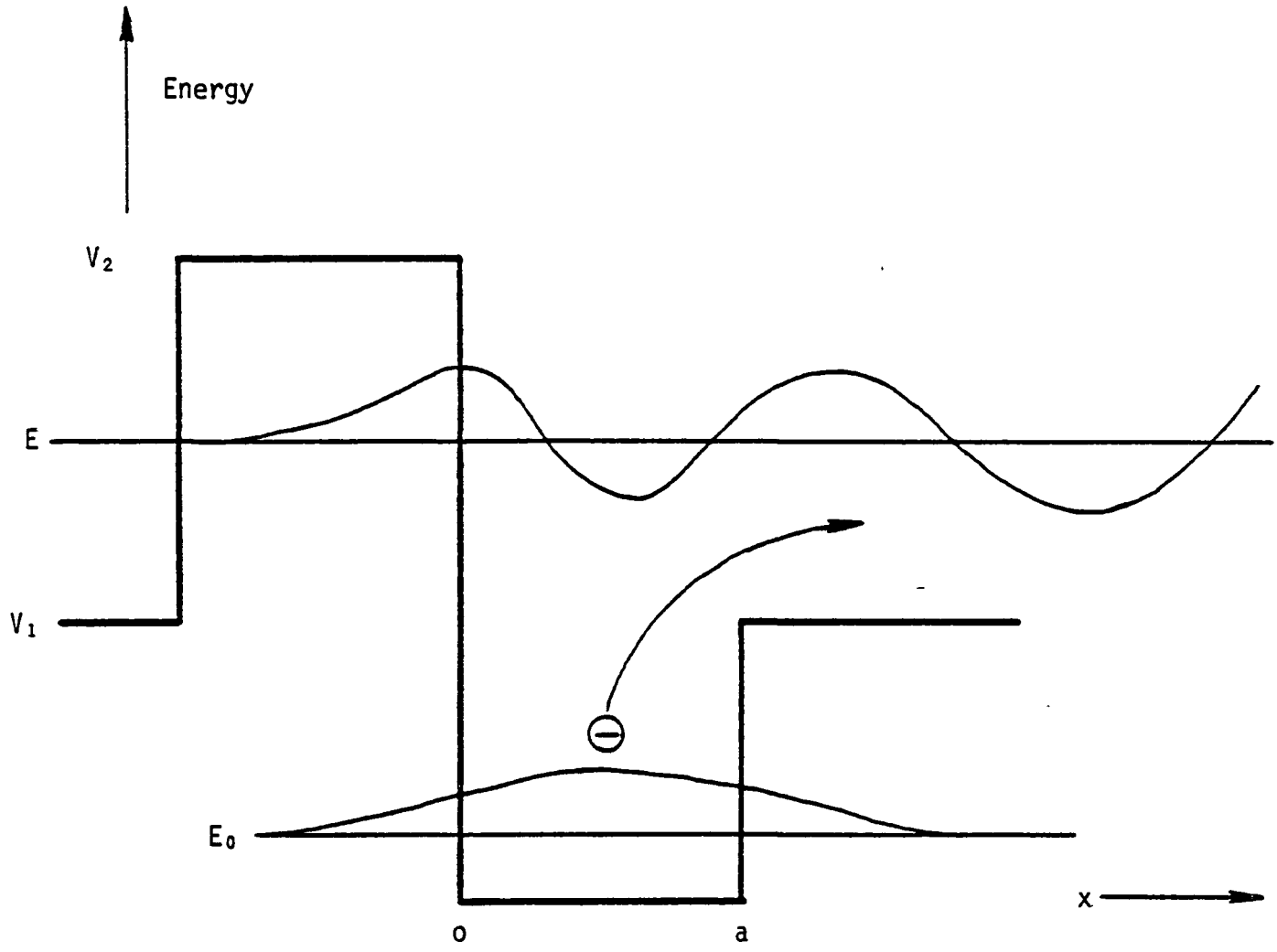

Figure 4. Electron photoexcited from anistropic trap. The ground state and excited state wave functions are shown (Glass et al model).

energy $V_1 < E < V_2$. The electron can freely move only in one direction (right side) because the potential barrier restricts its motion in the opposite direction. Since the asymmetry of the potential well maintains the same sense at all equivalent defects (due to the existence of a polar axis in the crystal), this results in a directional excitation current of the form

$$J = \frac{e\alpha I}{h\nu} P_+ l_+ - P_- l_- + z_i \Delta l_i \qquad (2)$$

where I is the incident intensity, α the absorption coefficient, P_+ and P_- are respectively the probability for electron transfer in the positive and negative polarization directions, and l_+ and l_- are the corresponding electron mean free paths in the two directions. The term $\zeta_i \Delta l_2$ accounts for the current produced by the displacement of Δl_i of the ionized impurity (of charge ez) that remains after the photoelectron has been excited. The steady state photocurrent is then calculated by taking the difference between the excitation current and the recombination current that arises when the excited electrons are retrapped, i.e.

$$J = J_e - J_r = k\alpha J \qquad (3)$$

where

$$K = \frac{e}{h\nu} P_+ l_+ - P_- l_- + P_+' l_+' - P_-' l_-' + Z_i \Delta l_i - Z_i \Delta l_i'$$

is a constant depending only on the nature of the absorbing center, the local environment, and the photon energy. The primed quantities are all parameters of the recombination process.

When an external potential is applied, a macroscopic electric field e_i is established inside the ferroelectric and the resultant current is given by

$$J = K\alpha I + \sigma E_i \tag{4}$$

where σ is the electrical conductivity of the illuminated sample. The open-circuit saturation voltage is readily obtained by setting $J = 0$, and integrating the resultant field over the length of the sample d.

$$V_{\Delta c} = - E_i D = \frac{+K\alpha I}{\sigma} d \tag{5}$$

Thus, even though the photoeffect may be small, in the sense that it might give rise to a small short-circuit photocurrent, the open-circuit voltage can be large, provided the sample conductivity is low.

RESULTS AND DISCUSSION

In this section , the structural characterization of the deposited films, the dielectric and C-V measurements, and the polarization-electric field (P-E) hysteresis loops used to confirm the ferroelectricity in the deposited films are discussed.

A major part of this research was concerned with attempts to reproduce the ferroelectric films of $BaTiO_3$ reported earlier [2, 3]. The ferroelectric layers were formed by rf sputtering in O_2/Ar mixture onto silicon substrates. A few runs were also performed with quartz substrates. These investigations on both n and p type samples and quartz substrate are discussed in this section. The ratio of oxygen to argon present during the deposition varied from 1:20 to 1:1 with no difference regularly observed in the composition of the resulting films. However, the stability of the glow discharge decreased as the percentage of O_2 was increased. It was qualitatively also observed that small variations in the amount of oxygen relative to the amount of

argon present made a large difference in the deposition rate for $BaTiO_3$. The lower the oxygen, the higher the deposition rate. Because of the instability of the glow discharge and the uncertainty of the deposition rate, and also because of the progressive deterioration of the pumping system with a gas mixture with a large amount of oxygen, the smallest reproducibly measurable amount of oxygen relative to argon, i.e., 5% O_2 was used regularly.

Structure

The structure of the $BaTiO_3$ films deposited on silicon was studied by the x-ray diffraction technique. In addition, the present study used the plane (100) of silicon instead of the (110) or (111) plane because only the (100) reconstructs to a Cartesian grid of surface atom sites; these could possibly act as nucleating sites to promote the growth of tetragonal or cubic $BaTiO_3$ [9, 10].

Figure 5 shows the typical x-ray diffraction patterns of sputtered films as well as the source material in which (a) is for a film (about 0.23 μm) sputtered on silicon at 55°C substrate temperature, (b) is for the film (0.5 μm) sputtered at 550°C substrate temperature, and (c) is for the source material. The diffraction pattern of the source material shows a good agreement with the tetragonal structure of $BaTiO_3$ in the ASTM data indexing card[11]. The lattice constants obtained are a = 4.002Å, c = 4.023 Å, and c/a = 1.005. Though the detailed crystal structure of bulk $BaTiO_3$ is well documented, the diffraction angle 2θ, the corresponding interatomic distance d, and the intensity ratio I/I_0 are reported in Table 1, so that these can be compared with those obtained for the film. Figure 5(b) is the x-ray diffraction pattern for a good film sputtered on silicon at 550°C substrate temperature. The parameters calculated from the peaks in the film show a good agreement with the target material. The

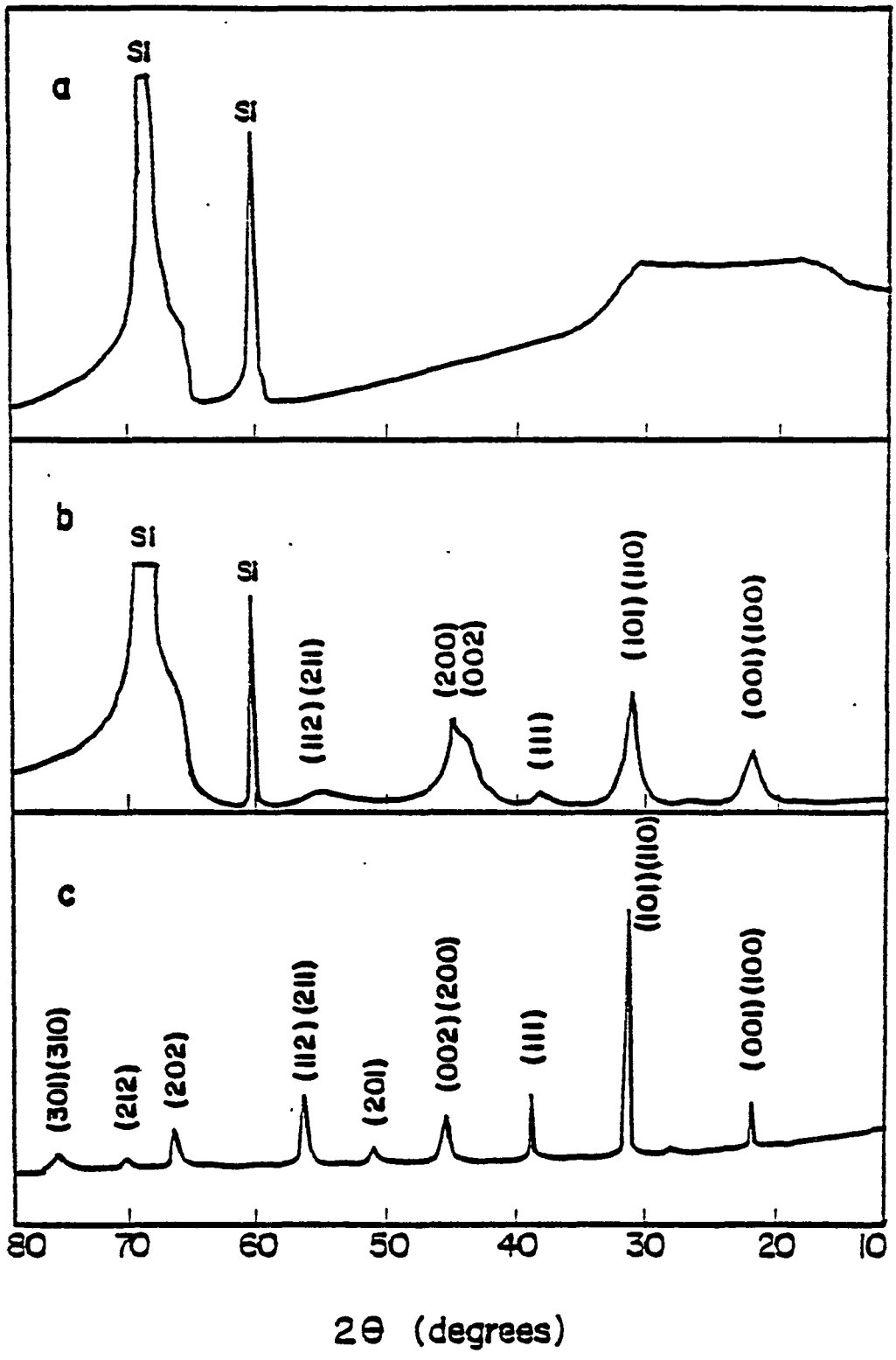

Figure 5. X-ray diffraction patterns of sputtered films and source material, using Cu Kα 1 radiation. (a) film sputtered on single-crystal silicon at substrate temperature of 55°C; (b) film sputtered at a substrate temperature of 550°C; and (c) source material.

lattice constants obtained are a = 4.006 Å, c = 4.080 Å, and c/a = 1.018. The half width of each peak in the film is, however, broader than that of the target. This broadening of the peak in the film is attributed to their small grain size and internal stresses in the film. The x-ray diffraction pattern for a film sputtered at 55°C (Figure 5a) gives a single broad diffuse peak, indicating that the film was amorphous, i.e., noncrystalline. From these results we can conclude, qualitatively, that the crystallinity of the sputtered films is mainly controlled by the substrate temperature. At room temperature, the films are amorphous; at temperatures higher than 500°C, the films exhibit a crystalline texture; and, its characteristics are closely resemble the tetragonal perovskite structure which usually has ferroelectric properties. The peaks at $2\theta = 61.8°$ and 69.50° in the sputtered films (Figure 5a and b) are due to silicon substrates. The structure of $BaTiO_3$ grown on fused quartz substrate at 600°C substrate temperature is shown in Figure 6. Here again the agreement between the two patterns is good. The surface structure of the films was examined by a scanning electron microscope. The micrographs revealed that the surface structure consisted of grains approximately 400 to 800 Å in diameter (Figure 7).

Dielectric and C-V Measurements

The capacitance was measured as a function of temperature at 1 MH_2 to make the ferroelectric phase transition. Figure 8 shows the temperature characteristics of capacitance for two different film thicknesses of $BaTiO_3$ sputtered on silicon. Curve (a) is for a film of about 0.3 μm thickness sputtered at 570°C substrate temperature. A broad transition in the region of 120°C is seen. Curve (b) represents the variation in capacitance with temperature for a film of about 0.5 μm thickness, whose x-ray diffraction pattern is given in Figure 5(b). A clear but broad peak is

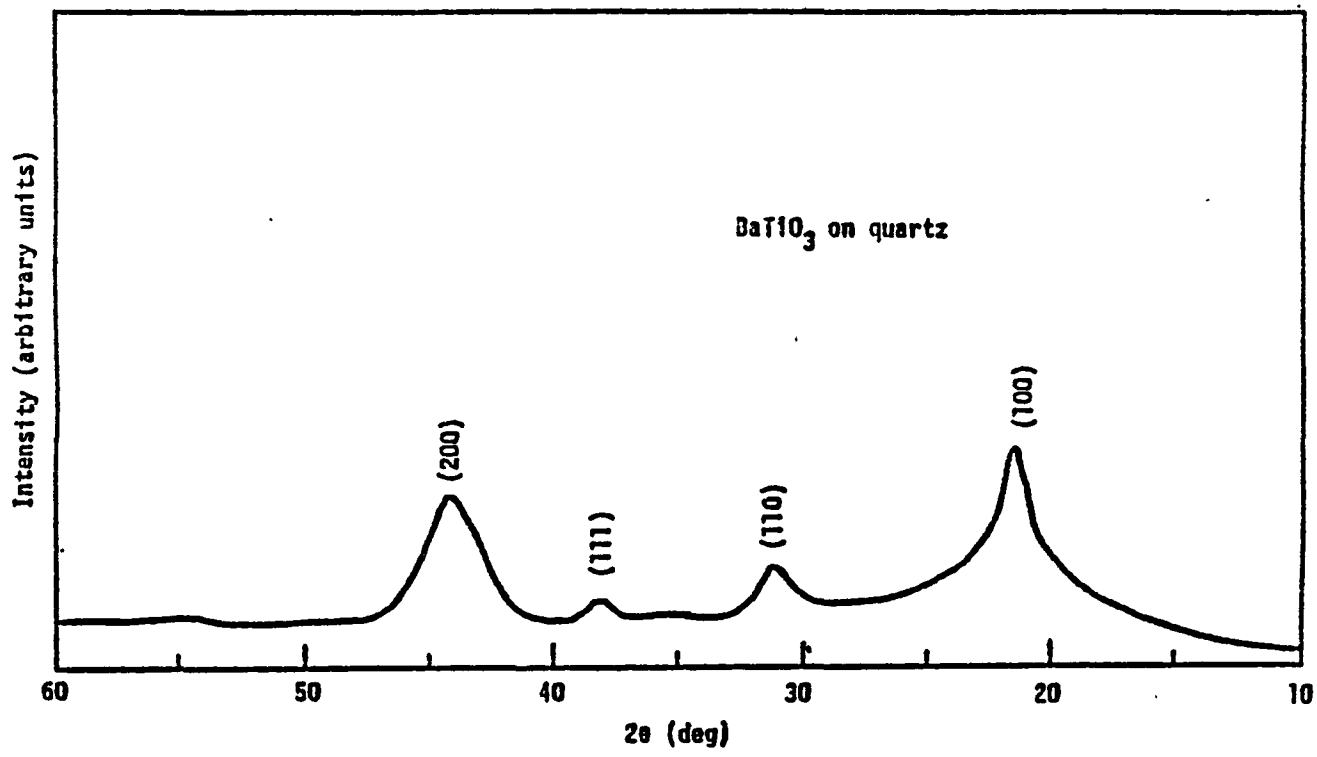

Figure 6. X-ray diffraction pattern of $BaTiO_3$ film on fused quartz.

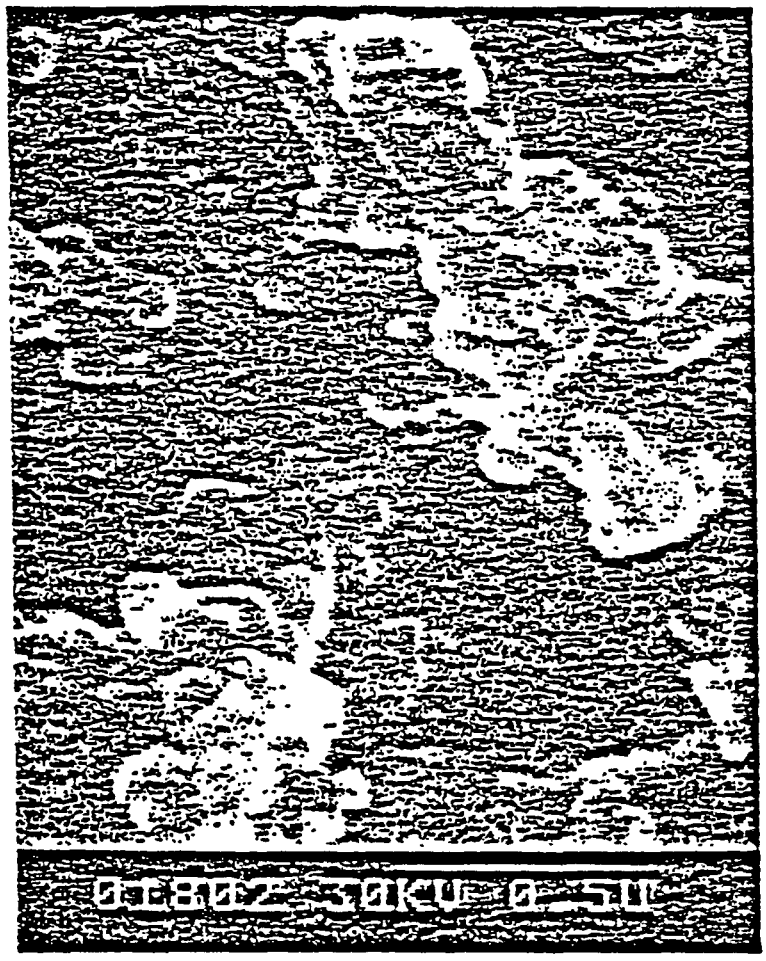

Figure 7. Scanning electron micrograph of $BaTiO_3$ film deposited on n-Silicon at substrate temperature of 500°C, magnification 50,000X times and L = 0.3 μm.

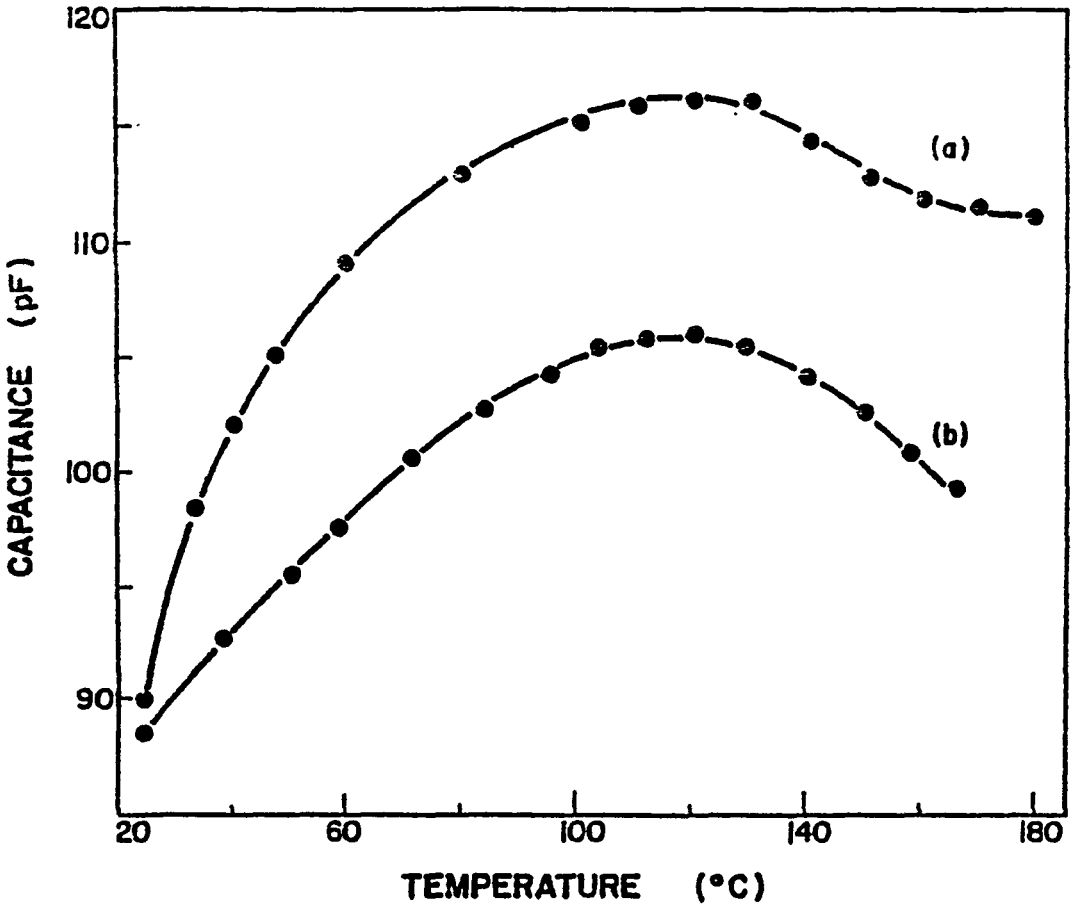

Figure 8. Capacitance vs temperature for two different film thicknesses of $BaTiO_3$ on silicon deposited at a substrate temperature of 550°C. These samples also exhibit a counterclockwise hysteresis CV curve at 1 MHz.

observed. Such smearing out of capacitance as a function of temperature is not unusual since similar effects have been reported earlier for thin films of $BaTiO_3$ [1, 2] and PZT [12]. Okazaki and Nagata [13] also observed similar effects in PLZT thin films and attributed the behavior to small grain size. They noted that the dielectric constant transition temperature was directly proportional to the grain size and explained these results on the basis of the space-charge model for PLZT. It appears from Figure 8 that the maximum value of the capacitance increases and the capacitance peak broadens as the film thickness decreases. The average grain size determined from the micrographs for the film in curve (a) is ~ 800Å. The smaller grain size of the film in (a) also contributes to peak broadening.

The smearing out of the C versus T curve can also be correlated with film thickness. Since the film is deposited onto a substrate whose coefficient of thermal expansion differs from that of the film, this will give rise to thermal stresses in the film when the substrate is cooled from the deposition temperature to room temperature. These stresses rise exponentially with decreasing film thickness. In our study in order to minimize mismatched coefficients of thermal expansion of Si (2.5×10^{-6}/°C at 20°C) and $BaTiO_3$ (8×10^{-6}/°C at 20°C), the substrates were cooled at a rate of about 6 to 7°C/min during the last part of the deposition [2]. In this report, therefore, when a substrate temperature above 200°C is mentioned this cooling procedure was followed. The temperature of the substrates was typically 160 to 200°C when the deposition ended. Films deposited at constant substrate temperatures above 200°C were electrically leaky.

The capacitance-voltage measurements at 1 MHz were also employed to study the ferroelectric effect and memory switching

properties of the films deposited under various deposition parameters. When tunneling or ferroelectric effect becomes important, the C-V curve opens up into a hysteresis loop with a clockwise or counterclockwise sense. Figure 9 shows the typical C-V curve obtained for $BaTiO_3$ film on silicon, whose x-ray diffraction pattern is given in Figure 5b. The counterclockwise sense of the curve with a hysteresis window of about 9 V for a ±15 V bias clearly shows the ferroelectric effect in the films.

The physical mechanism associated with the counterclockwise hysteresis loop is as follows. If we suppose that the ferroelectric of a metal-ferroelectric-semiconductor structure originally has its polarization pointing towards the ferroelectric-semiconductor interface, the remanent polarizaton will then induce a field which will attract negative charges to the semiconductor surface. For an n-type semiconductor, this will create an accumulation layer and for a p-type semiconductor, a charge depletion layer. Similar behavior is observed when the polarization direction is reversed, i.e., away from the ferroelectric-semiconductor interface. The field induced by remanent polarization, in this case, will repel the negative charges and attract the positive charges to the semiconductor surface. The carrier density of an n-type semiconductor at the interface will be depleted and that of the p-type will be enhanced. If there is no remanent polarization in the film, the C-V curve will not exhibit hysteresis. The effect of the remanent polarization is shown by the shift of the flat band voltage [14], depending on the polarization direction.

Figure 10 shows a set of C-V curves obtained for the same device of Figure 9. After recording the original C-V curve, a set of curves was obtained by successively applying positive write pulses with increasing duration and amplitude until the device has switched to a flat-band position near the positive

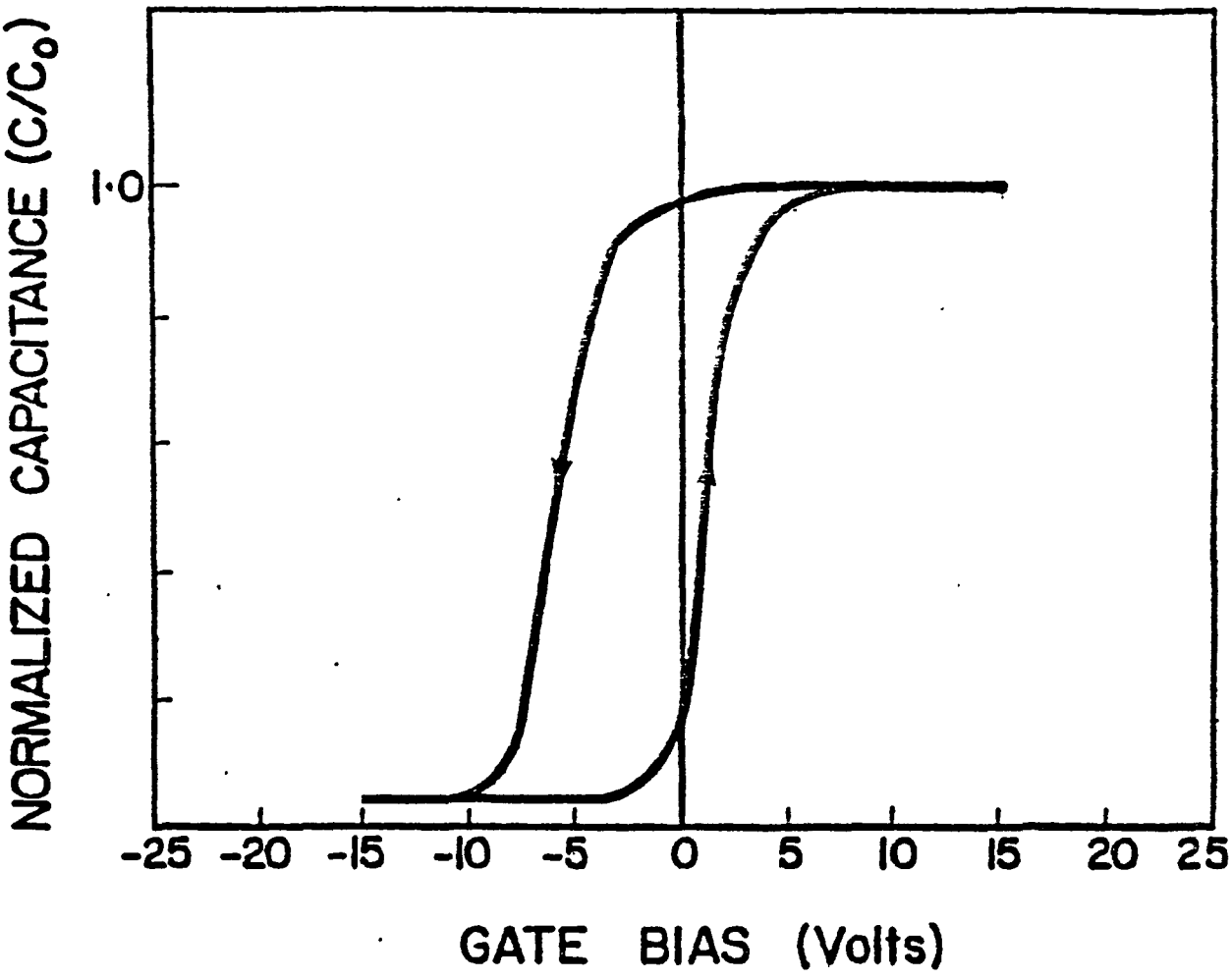

Figure 9. Typical ferroelectric hysteresis curve for $BaTiO_3$ film deposited on silicon at substrate temperature of 550°C, 1 MHz.

Stress Sequence
(volts/msec)

1) Original
2) -20, 10
3) -25, 10
4) -30, 10
5) +20, 10
6) -25, 10
7) +15, 10
8) +15, 50
9) +15, 100
10) +20, 10
11) +20, 100
12) +25, 10
13) +25, 50
14) +25, 100

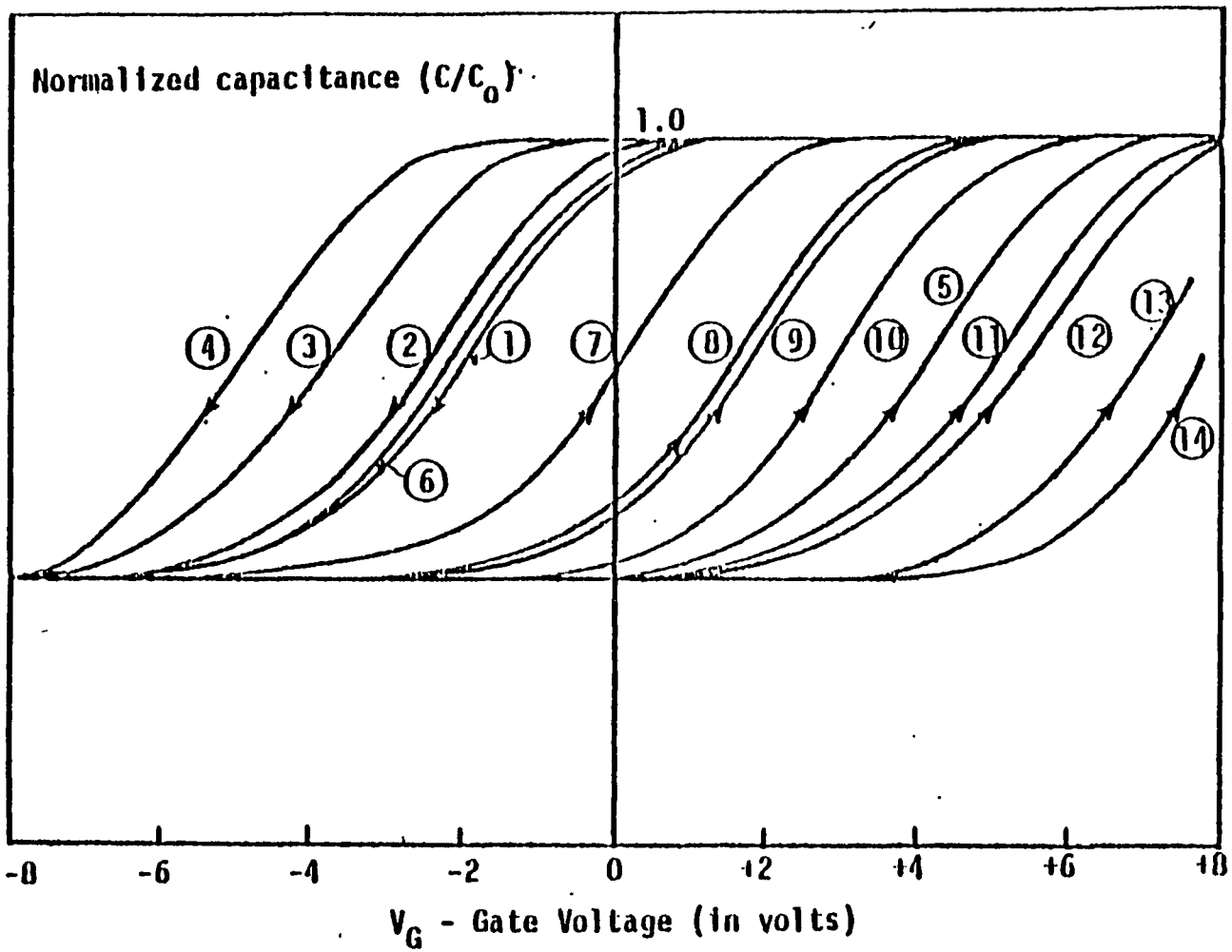

Figure 10. C-V memory switching characteristics of $BaTiO_3$ films deposited on silicon at substrate temperature of 550°C, 1 Mhz.

bias end. Then the device was switched to the negative direction by successively applying negative bias pulses. Thus, this particular device can be effectively switched to the positive end by approximately +25V; a 50 msec pulse and a -30V pulse are needed to switch to the negative end.

Polarization-Electric Field Hysteresis (P-E) Measurements

Polarization (P) is a measure of the degree of ferroelectricity. The $BaTiO_3$ films were confirmed to be ferroelectric at room temperature from the observation of the P-E hysteresis loops by means of a Sawyer-Tower circuit. Figure 11 shows a family of 60 Hz hysteresis loops obtained from a 0.5 μm, film deposited on silicon at 550°C. This is the film with tetragonal structure whose x-ray diffraction pattern was given in Figure 5b. The hysteresis loops of Figure 11 indicate that the saturation polarization was not attained with the field amplitudes applied, since the polarization continued to increase with increasing sinusoidal switching field. This effect results from the specific properties of the silicon/sputtered $BaTiO_3$ film. Between the silicon and the sputtered ferroelectric film, an intermediate layer with a markedly distorted crystal lattice exists. The strong domain fixing in this intermediate layer, which has a high concentration of defects, hinders the switching process. With an increase in the amplitude of the switching field, the number of domains switching also increases causing an increase in the maximum value of P determined from the experimental hysteresis loop. The presence of an intermediate layer has been established from layer-by-layer analysis of the Auger Spectra of the ferroelectric $BaTiO_3$/silicon system. These AES results will be presented in a later section on Guger Analysis.

The polarization (P) and the coercive field (E_c) obtained from the largest loop (Figure 11) are 1.10 $\mu c/cm^2$ and 70 kV/cm respectively. Figures 12a-12c show the change in the shape of

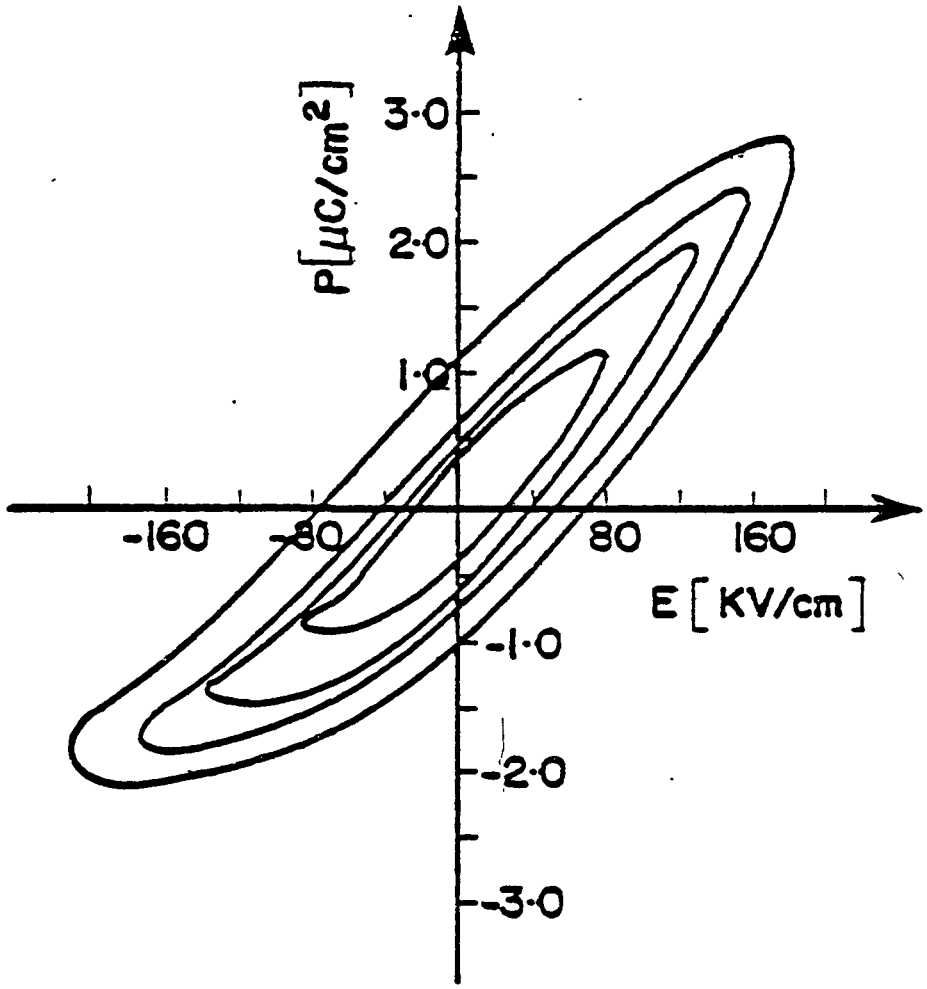

Figure 11. P-E hysteresis loops for 60 Hz sine wave at four amplitudes of 3.9, 6, 8, and 14 V.

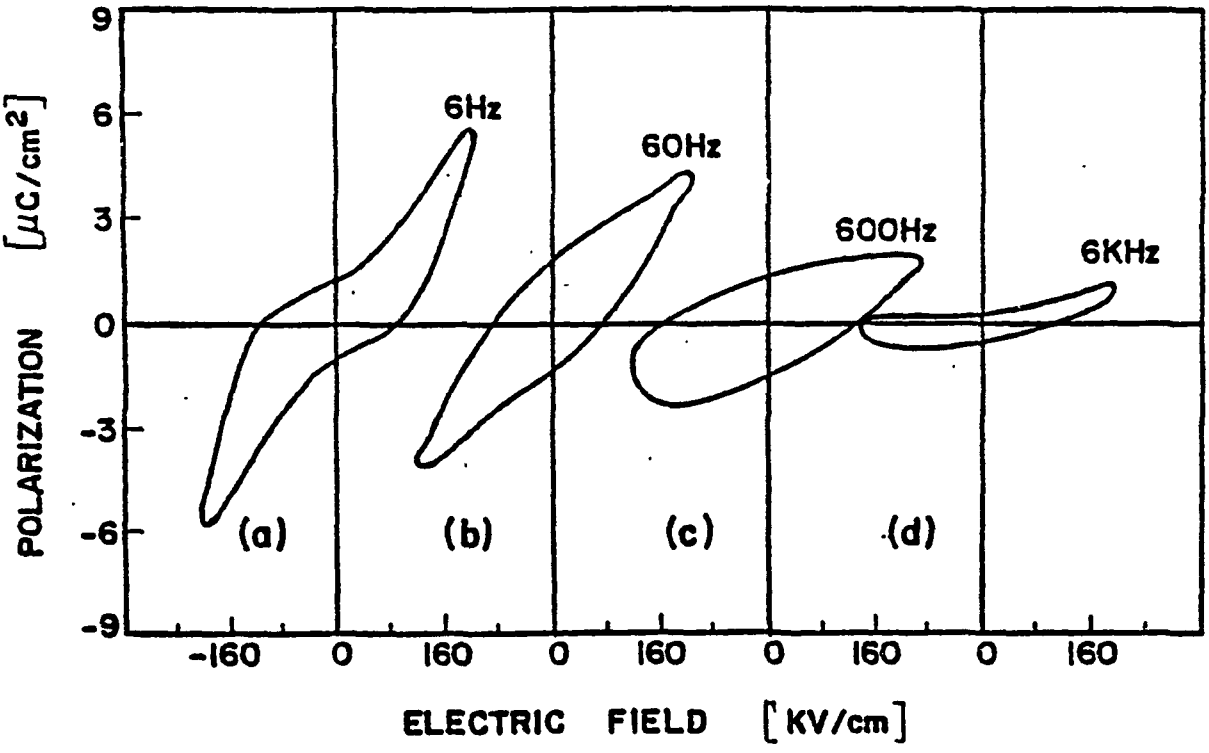

Figure 12. P-E hysteresis loops for sine waves with an amplitude of 4 V. The frequencies are (a) 6 Hz, (b) 60 Hz, (c) 600 Hz, and (d) 6 kHz. The film thickness is 0.3 μm.

the P-E hysteresis loop with frequency, for the same MFS device tested in Figure 8a. The frequencies are 6, 60, 600 and 6 kHz for Figures 12a, 12b, 12c, and 12d, respectively. The origin was shifted along the horizontal axis from left to right for clarity. The measured P and E_c at 60 Hz for this device are 2.0 $\mu c/cm^2$and 72 kV/cm, respectively. The low P and high E_c compared to the bulk material may be attributed to the small-grain size surface layer at the ferroelectric-semiconductor interface.

The P-E hysteresis loop for a $BaTiO_3$ film (0.5 μm) grown on fused quartz substrate at 600°C substrate temperature, is shown for Figures 12a, 12b, 12c, and 12d, respectively. The origin was shifted along the horizontal axis from left to right for clarity. The measured P and E_c at 60 Hz for this device are 2.0 $\mu C/cm^2$ and 72 kV/cm, respectively. The low P and high E_c compared to the bulk material may be attributed to the small-grain size surface layer at the ferroelectric-semiconductor interface.

The P-E hysteresis loop for a $BaTiO_3$ (0.5μm) grown on fused quartz substrate at 600°C substrate temperature, is shown in Figure 13. This is the film whose x-ray diffraction pattern is given in Figure 6. The film was grown under identical deposition conditions to the film grown in Figure 11, except that in this case indium tin oxide (ITO) films were used as the electrodes. A high polarization value of 48 $\mu C/m^2$ and a relatively low coercive field of 220 kV/cm is obtained. These results again support the speculation of the presence of an intermediate layer at the $Si/BaTiO_3$ interface which poisons the ferroelectric properties. The high value of P in this case as compared to films formed on silicon shows that probably no interaction between the substrate film is taking place.

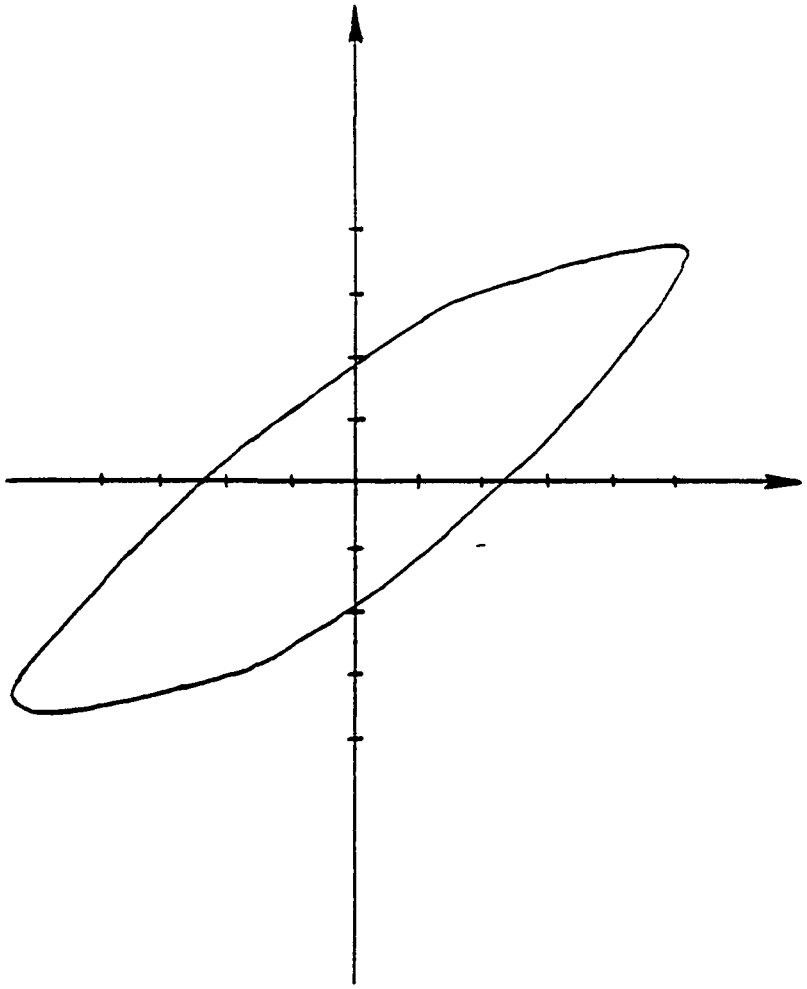

Figure 13. P-E hysteresis loop for 60 Hz sine wave at an amplitude of 19 V for a 0.5 μm thick film deposited on fused quartz substrate at 600°C substrate temperature.

PHOTOVOLTAIC EFFECT

In addition to studying the ferroelectric properties, the photovoltaic properties of the devices were also studied. These studies are documented in this section.

A series of measurements of short-circuit photocurrent and open-circuit photovoltage were made in an effort to understand the mechanism associated with the photoferroelectric effect in the $BaTiO_3$/silicon system. No reported study of any kind on thin film $BaTiO_3$ exists in literature, and no determination of the basic properties such as short-circuit photocurrent, open-circuit photovoltage, transient photocurrent, etc. have been published, adding further importance to such an investigation.

When a device is illuminated with near-UV light without any applied field, at least two important physical effects can take place [15].

1. Photoexcitation of carriers both from the trapping centers in the $BaTiO_3$ band gap and across the band gap by near-UV light of energy equal to or greater than the band gap.

2. Carriers photoexcited to the conduction state diffuse (with no field applied) or drift under the influence of an applied field to new trapping sites beyond the absorption depth of the $BaTiO_3$. Retrapped carriers establish a space charge field E_{sc}. Carriers remaining in the conduction state contribute to a steady-state photovoltaic current I_{pv}, which is driven by the bulk photovoltaic effect [8]. The photocurrents I_{sc} and I_{pv} both exist in the domain nucleation and thus help the domain switching process.

3. A transient photocurrent I_{sc} is associated with the photoexcited carriers which are retrapped to establish

E_{sc}. Carriers remaining in the conduction state contribute to a steady-state photovoltaic current I_{pv}, which is driven by the bulk photovoltaic effect [8]. The photocurrents I_{sc} and I_{pv} both exist in the domain nucleation and thus help the domain switching process.

In addition to the effects enumerated above, since poled ferroelectric $BaTiO_3$ is also pyroelectric, photon absorption produces a temperature rise which results in a transient pyroelectric current I_{py}.

If the device is short-circuited and one of the surfaces of $BaTiO_3$ is illuminated with near-UV light, all components of the photocurrent I_{hv} are proportional to the light intensity I. This effect is illustrated in Figure 14 which shows I_{hv} plotted as a function of time. The curve shows the transient I_{py} and the steady-state I_{pv} for the light-on condition and the transient I_{py} for the light-off condition. From about 20 to 35 seconds, the curves represent the steady-state I_{pv}. The steady-state I_{pv} is proportional to the absorbed light intensity, I.

$$I_{pv} = K\alpha I \tag{6}$$

This is illustrated in the inset of Figure 15.

Under open-circuit conditions, the photocurrent charges the $BaTiO_3$ capacitance generating a macroscopic electric field E_i given by

$$J = K\alpha I + \sigma E_i \tag{8}$$

Since $\sigma \alpha I$, I/σ is a constant and the open-circuit steady state photovoltage during illumination is constant,

$$V_{oc} \; E_{sat}{}^{d} \tag{9}$$

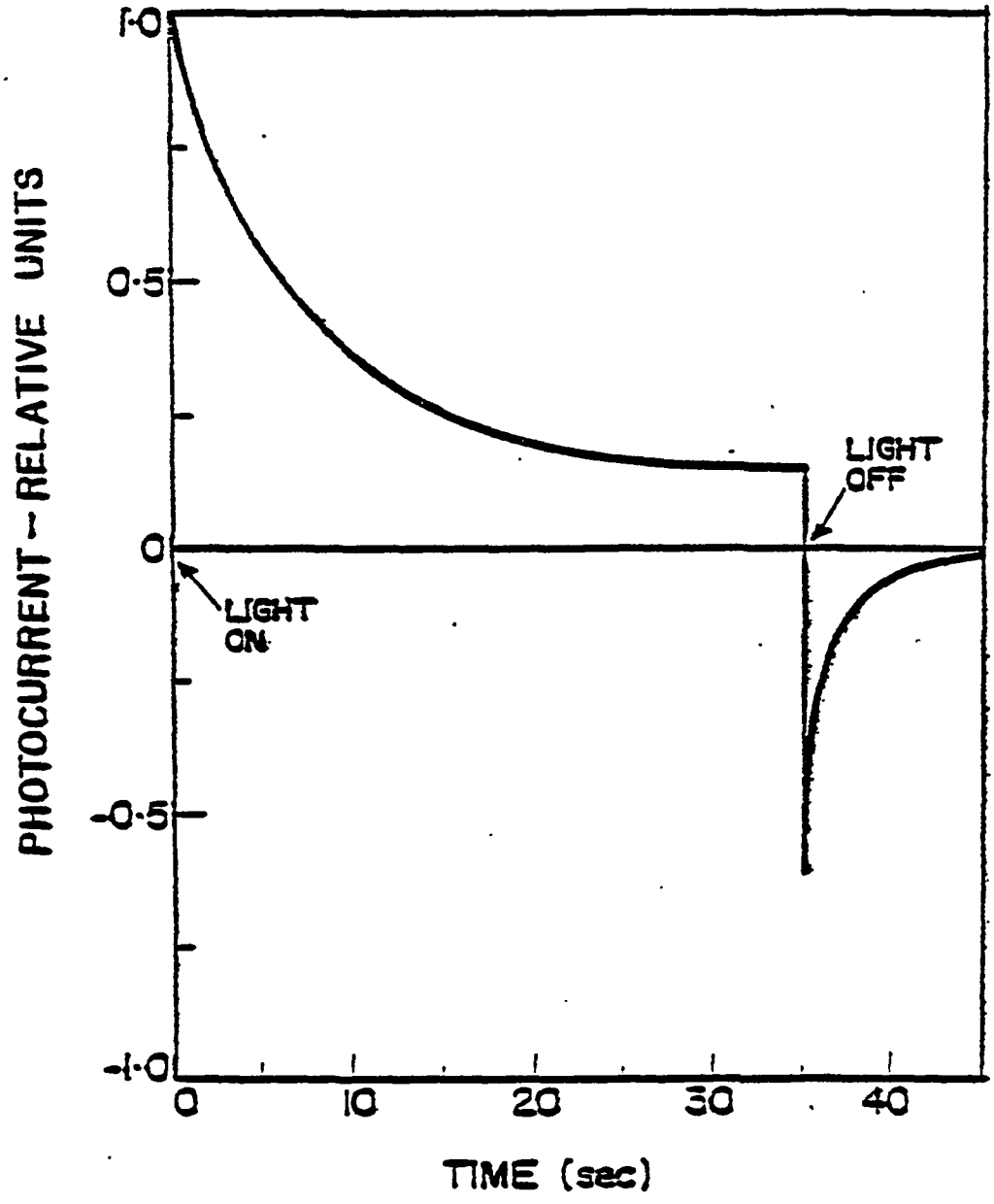

Figure 14. Short-circuit photocurrent in $BaTiO_3$ thin film as a function of time.

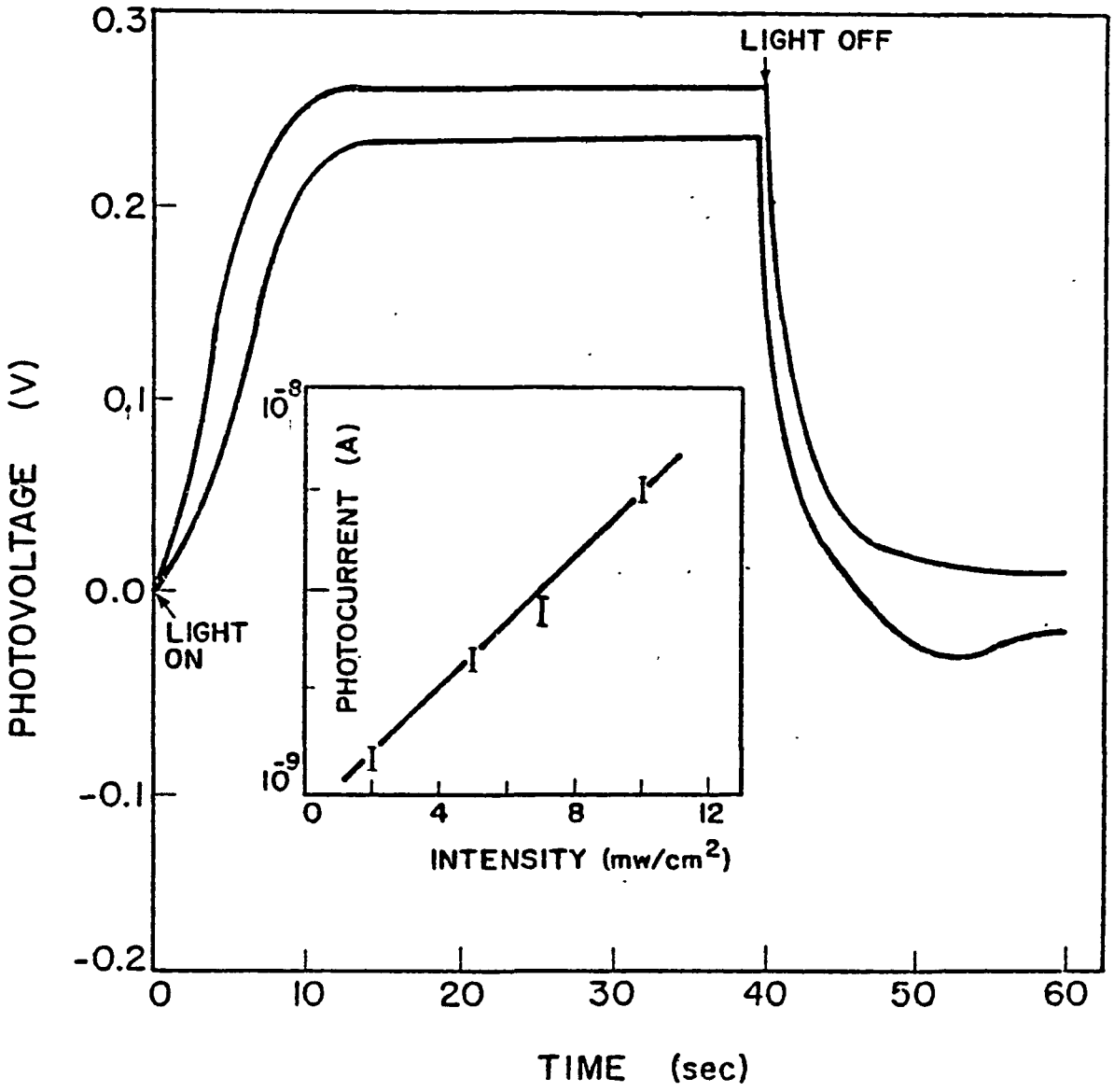

Figure 15. Open-circuit photovoltage as a function of time for two different $BaTiO_3$ film devices. The inset shows the photocurrent (I_{pv}) versus light intensity.

where d is the $BaTiO_3$ film thickness. This result is presented in Figure 15. The transient voltages from 0 to 15 seconds are due to a transient pyroelectric charge V_{py}. From about 15 to 40 seconds, at which time the light is turned off, V_{oc} is a constant independent of intensity, I. When the light is turned off, the transient voltage V_{py} decays to zero with the dielectric relaxation time of the material.

Open-circuit saturation voltages (V_{oc}) corresponding to fields of about 24 kV/cm are observed in $BaTiO_3$ films. For intensities greater than 7 mW/cm^2, the open-circuit saturation field is independent (Figure 16) as expected from Equation 9. Further, we also observed the photovoltage to increase as the poling voltage was increased, until the polarization saturated. However, the magnitude of the photovoltage in the two directions of the polarization was quite different. Also, the photovoltage slowly decayed with time to lower values. These deteriorating features are probably due to the presence of the intermediate layer. Therefore, we decided to characterize the films and their interfaces with the substrate to have a better understanding of the observed results.

AUGER ANALYSIS

As discussed in the previous section, the chemical composition of the sputtered films were investigated using scanning Auger microscopy combined with argon-ion in depth profiling. The results obtained from such study are discussed in this section.

Typical AES spectrum for the $BaTiO_3$ films deposited on silicon substrates maintained at temperatures ranging from 55 to 600°C and in the energy range between 0 and 2000 eV are shown in Figure 17. Figure 17a shows the spectrum taken on the surface of the film deposited on n-Si substrate held at room temperature. Figure 17b is for film deposited on n-Si at 580°C, while Figure

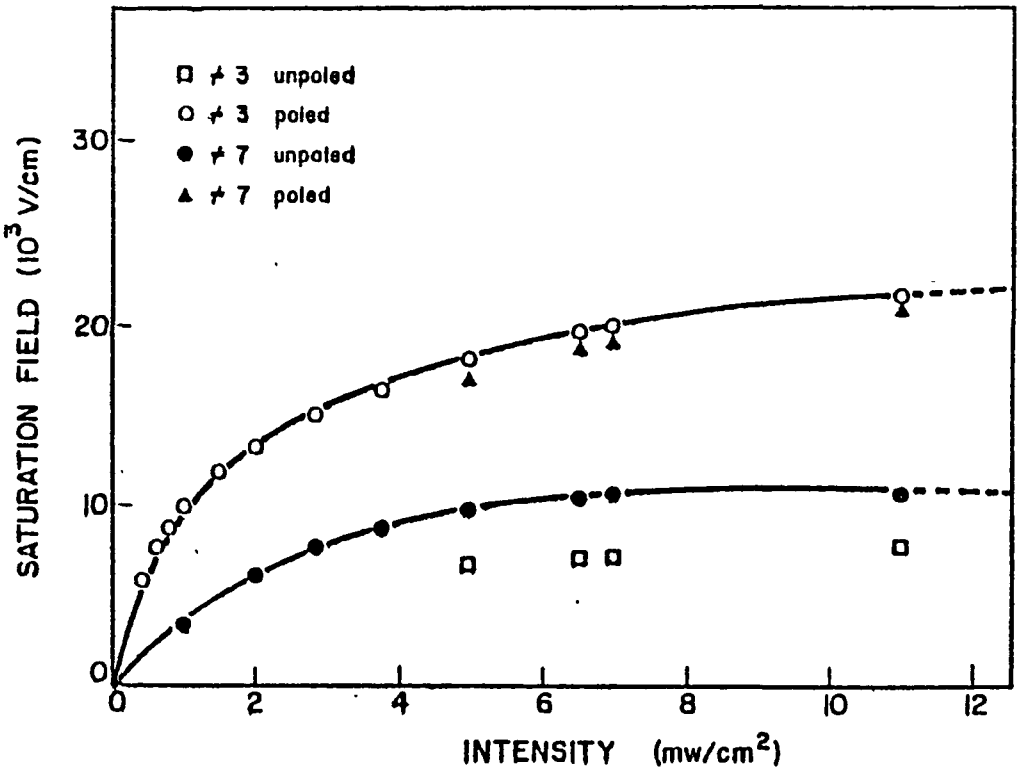

Figure 16. Open-current saturation field as a function of intensity of illumination for two devices under poled and unpoled conditions.

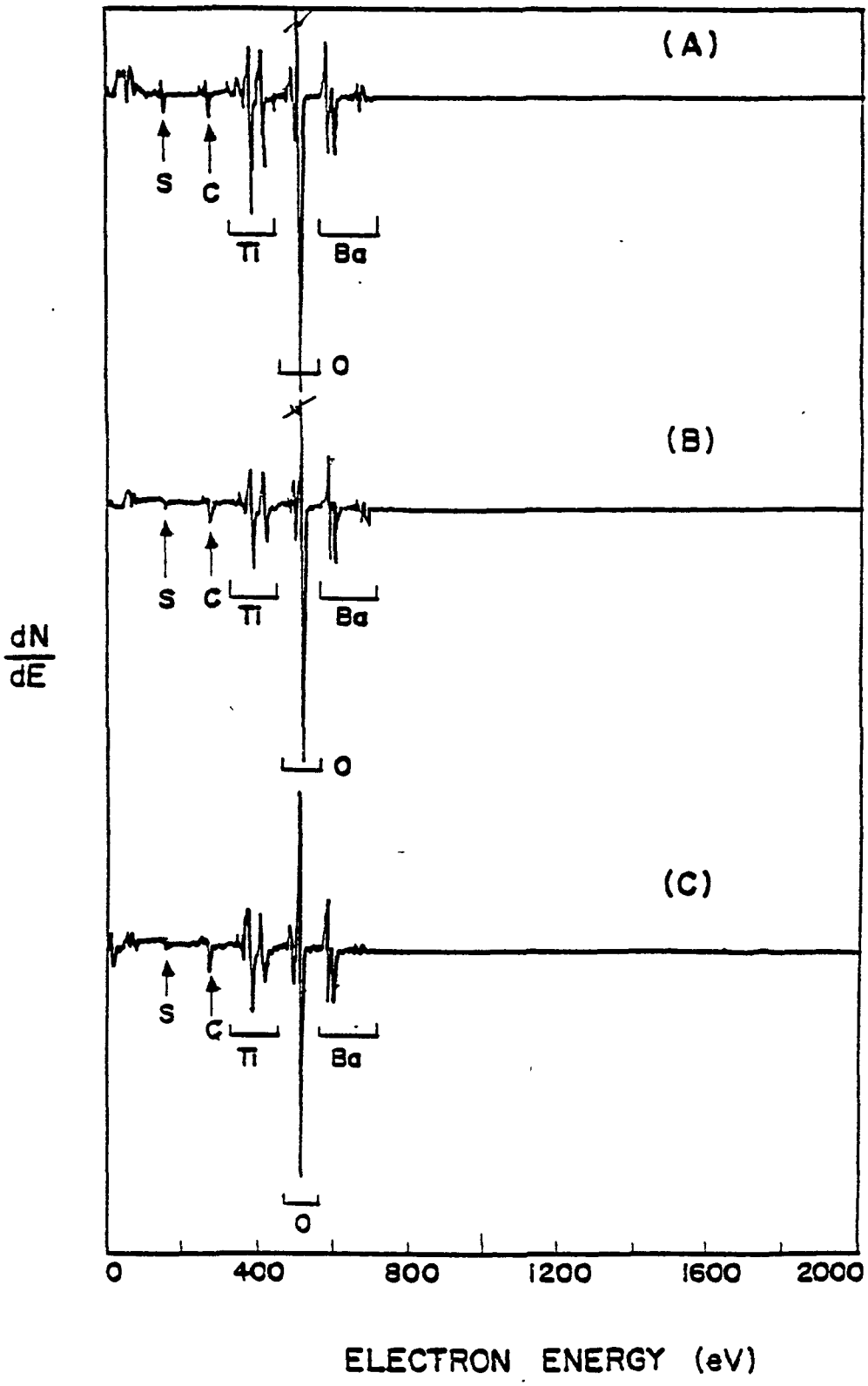

Figure 17. Auger survey spectrum from the surface of $BaTiO_3$ film sputtered on silicon substrate (a) n-Si; 55°C, (b) n-Si; 580°C, and (c) p-Si; 583°C.

17c is a spectrum taken for films deposited on p-Si at 583°C. In addition to the expected barium, titanium, and oxygen peaks, small amounts of carbon and sulphur impurities on the surface are present. The carbon signal probably results from the adsorption of carbon-containing atmospheric gases. Another source lies in hydrogen molecules forming part of the vacuum oil of the system in which the films were sputtered. The sulphur impurity could have been left after the standard cleaning procedure used in the device processing. However, a careful look at the shape of the carbon spectra shows that the carbon is predominantly in carbide form. No major changes in the AES spectra are found for films deposited at different substrate temperatures.

By recording peak-to-peak height as a function of removal of material by ion sputtering, the information about the depth distribution of the chemical elements in the sample can be obtained [16]. The chemical depth profiles of oxygen (KLL), titanium (LMM), and barium (MNN) through the $BaTiO_3$/silicon structures as a function of ion sputtering time are shown in Figures 18-20. The parameters are similar to those of Figure 17a-c, respectively. The cross section of the films contains three regions, an external surface layer, a main layer, and an intermediate film-substrate layer. The external surface contains an excess of barium. Apart from this, the surface layer has a considerable amount of adsorbed carbon, and hence oxygen combined with the latter. This aspect, as well as the deficit of Ti, causes an increase in the proportion of oxygen on the surface. The atomic concentration of the elements computed using a relative Auger sensitivity of the elements with respect to silver, according to the tables in the handbook of Auger Electron Spectroscopy from Physical Electronics [17] is shown in Table 2.

After removal of the surface layer the concentration curves (i.e., in the main layer) exhibit plateaus, the extent of which

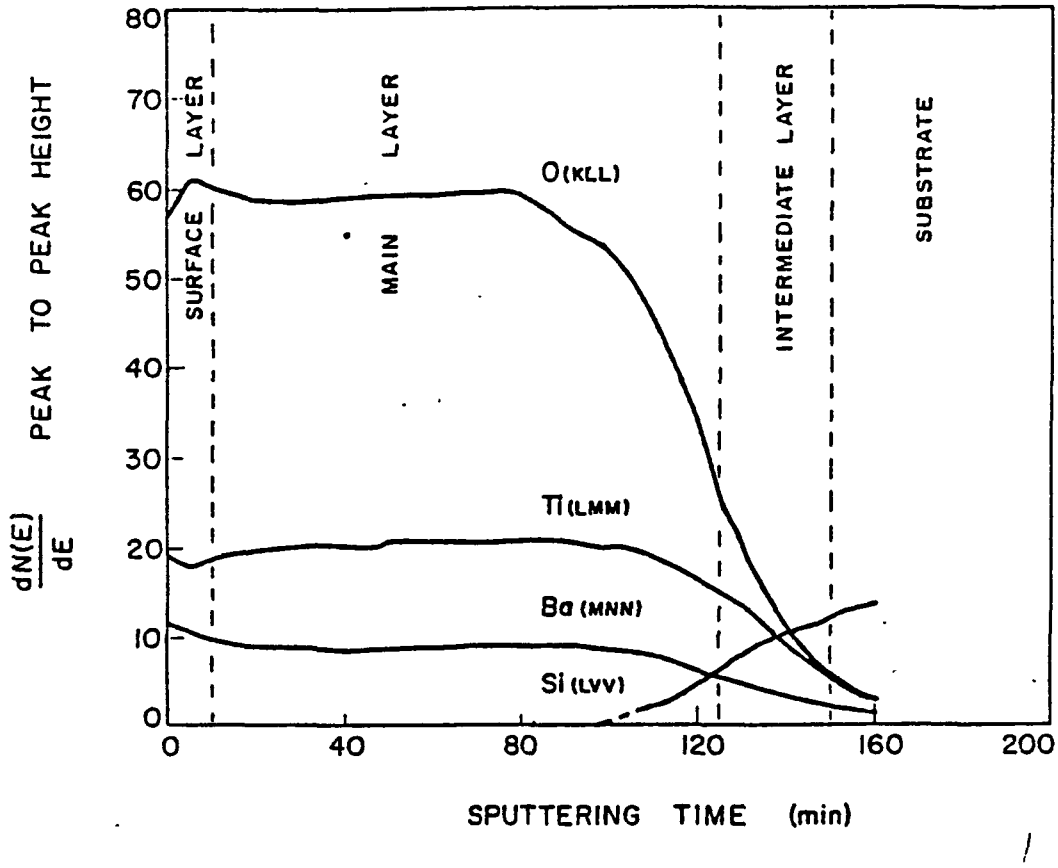

Figure 18. Derivative Auger depth profile through $BaTiO_3$ films sputtered on n-silicon (substrate temperature = 55°C; Ar/O_2 ratio = 95.5; deposition rate = 7 Å/min).

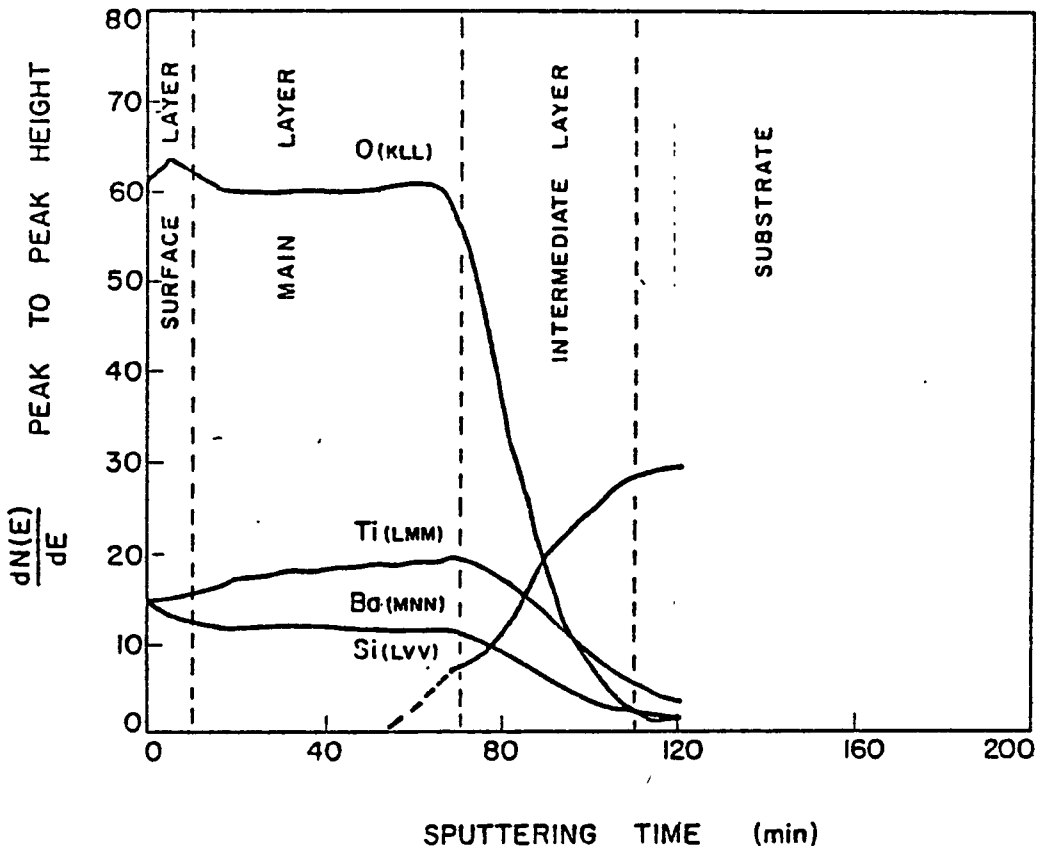

Figure 19. Derivative Auger depth profile through $BaTiO_3$ films sputtered on n-Si (substrate temperature = 580°C; Ar/O_2 ratio = 95.5; deposition rate = 5 Å/min).

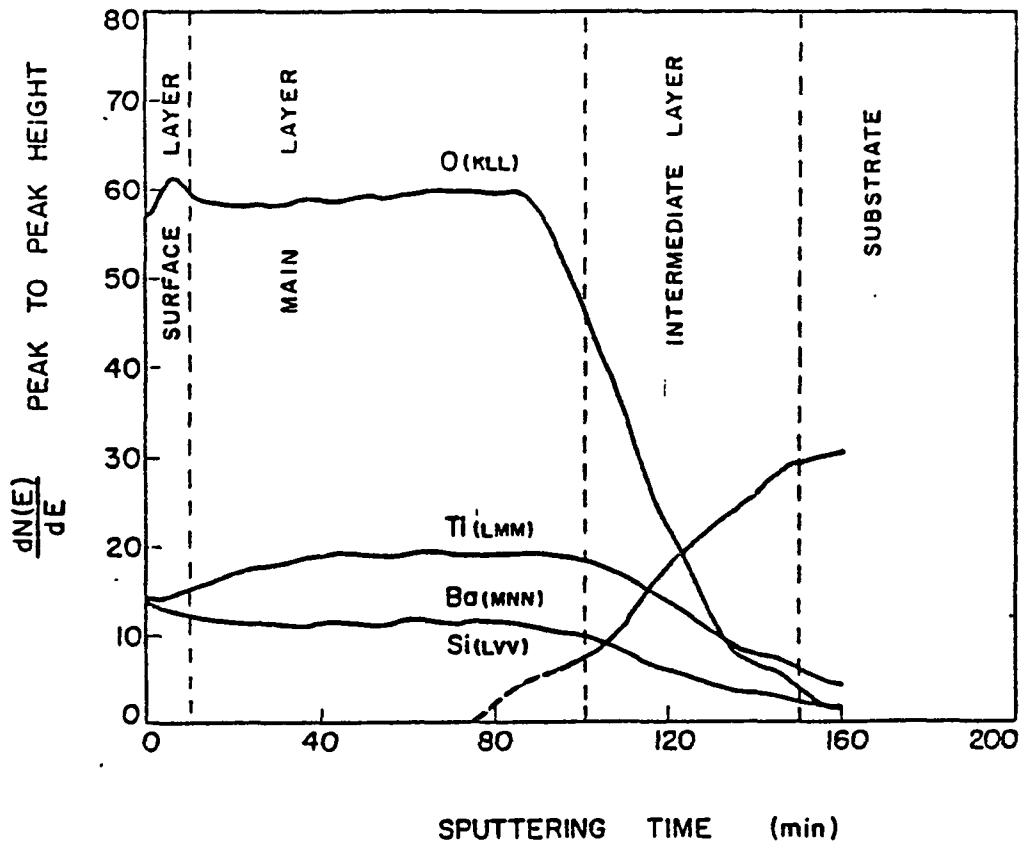

Figure 20. Derivative Auger depth profile through $BaTiO_3$ films sputtered on p-Si (substrate temperature = 583°C; Ar/O_2 ratio = 95.5, deposition rate = 6 Å/min).

is a function of deposition temperature. For films synthesized at room temperature, an excess of Ti, relative to films formed at high substrate temperature is observed.

The chemical depth profiles of the intermediate layer indicate that the $BaTiO_3$ interfaces are not abrupt but rather form a continuous region of varying chemical composition. More detailed analysis of the interface region shows the formation of reduced form of titanium dioxide $TiO_{2-x}(x < 2)$. The analysis also shows that SiO_x - $(x < 2)$ is formed. Another interesting feature observed is that the width of the intermediate layers, with other parameters constant, is a function of deposition temperature. The width of the intermediate layers is more for films formed at higher substrate temperature. Two possibilities can be considered: 1) the diffusion of Ba, Ti, and O into the substrate, and/or 2) the out-diffusion of silicon into the sputtered film. During the sputter deposition, electron and ion bombardment of the substrate occurs leading not only to heating but also to creation of point defects at the surface. Figure 21 shows the spectrum taken after the $BaTiO_3$ film has been sputtered out. Presence of Ti, Ba, and O is still observed. Of these the concentration of titanium is high. The presence of argon is due to argon atoms implanted during the sputtering process and is not an inherent impurity in the $BaTiO_3$.

Thus, experimentally, the formation of the following types of layers in rf sputtered $BaTiO_3$ films on silicon are observed:

1. an external surface layer containing carbon and an excess of barium up to a few tens of angstroms thick,
2. the main layer with stable composition, but the concentration is dependent on the evaporation condition, and
3. an intermediate film-substrate layer consisting of the components $TiO_{2-x}(< 2)$, and the interdiffusion of Ba, Ti, O, and Si. The formation of the TiO_{2-x} layer is

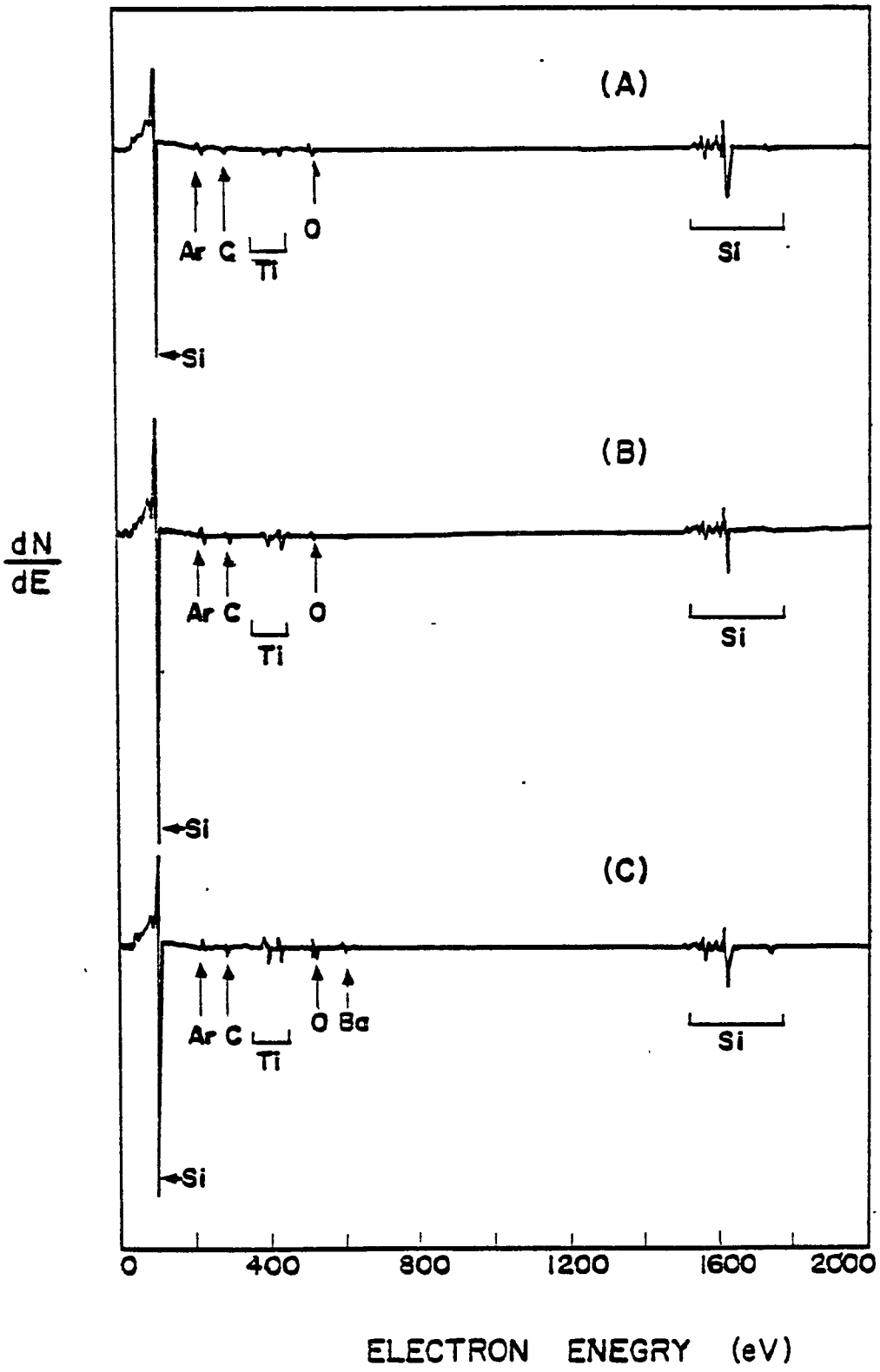

Figure 21. Typical Auger survey spectrum from the $BaTiO_3$/silicon interface after the $BaTiO_3$ film is sputtered out (parameters same as Figures 18-20, respectively).

due to the combination of high temperature and vacuum, which favors the reducing process. The adhesion coefficient of oxygen falls rapidly with increasing temperature which shifts the equilibrium of the reaction $Ba/tiO_3 = BaO + TiO_2$ to the right. On the other hand, the volatile BaO reevaporates with greater probability than TiO_2.

Jona and Shirane [4] have discussed the nature of surface layers of ferroelectrics and classified them on the basis of two models--space change layers due to ion vacancies, and layers formed by chemical or mechanical action which takes no part in the polarization reversal process, but will give rise to interface charges. Our experimental results are in favor of the second model.

EFFECTS OF SURFACE LAYERS ON FERROELECTRIC PROPERTIES

After having established the presence of intermediate and surface layers, it is worthwhile to examine the effects of these on certain ferroelectric parameters.

The thickness of the surface layer as determined from Auger analysis varied between 50-80 Å, whereas the intermediate film substrate layer thickness was a function of deposition temperature and was between 250-500Å. The contribution of these two layers to the dielectric constant of a three-layer capacitor with $BaTiO_3$ film as the dielectric can be obtained from (18).

$$\varepsilon_0 = \frac{l_0 \varepsilon_1 \varepsilon_2 \varepsilon_f}{l_f \varepsilon_1 \varepsilon_1 + l_1 \varepsilon_1 \varepsilon_f + l_1 \varepsilon_1 \varepsilon_f} \tag{10}$$

where l_0, l_1, l_2 and l_f are respectively the measured thickness and thicknesses of the surface layer (Type 1) intermediate film-substrate layer (Type 2) and of the ferroelectric itself; ε_1,

ε_2, and ε_f are the dielectric constants of these layers. Putting l_0 = 1500 Å, l_1 = 80 Å, l_2 = 450 Å, l_f = 970 Å, ε_1 = 5, ε_2 = 50. amd ε_f = 500, we obtain $\varepsilon_0 \sim 56$. This reduction in the dielectric constant of the ferroelectric film is observed in practice. These layers are not ferroelectric and therefore participate in screening the spontaneous polarization. This causes an increase in the coercive field. Further, these layers generally have a much higher impedance (lower dielectric constant) than the bulk (main layer) and also do not vary as rapidly with temperature near T_C as the main layer, thus broadening the phase transition so that there is no apparent discontinuity in the dielectric constant.

There have been a great many experimental observations which indicate that ferroelectric behavior at the surface of crystals differs from the bulk behavior. According to these data, the thickness of these surface layers is 10^{-4} to 10^{-6} cm with a low dielectric constant of the order of several units at the (001) surface in $BaTiO_3$. Also, there is a strong electric field 10 - 10 V/cm in the volume of this layer. According to Merz and Fatuzzo [4], this layer is a surface region of the crystal in which dielectric saturation and piezoelectric compression occurs because of the strong electric field. This causes a decrease in dielectric constraint in the surface layer. In the opinion of Triebwasser [19], the surface layer in $BaTiO_3$ is a Scholtky barrier formed with the contact of the $BaTiO_3$ with the electrodes.

In semiconductors the surface layers play a significant role in the formation of a barrier with contact of the semiconductor with a metal electrode. Solving Poisson's equation for one dimension in the space charge region of the semiconductor

$$-\frac{dE}{dx} = \frac{d^2\phi}{dx^2} = \frac{4\pi\rho(x)}{\varepsilon_s} \text{ where } \rho(x) = qN_d.$$

$$E = \frac{4\pi qN_d}{\varepsilon_s}\int_0^x dx = \frac{4\pi qN_d}{\varepsilon_s} + C_1$$

$$\text{at } x = d_i;\ e = 0 \rightarrow C_1 = \frac{-4\pi qN_d}{\varepsilon_s}$$

$$E = \frac{4\pi qN_d}{\varepsilon_s}(x - d_i)$$

$$\phi(x) = \frac{4\pi qN_d}{\varepsilon_s}\int_0^x (d_i - x)dx = \frac{4\pi qN_d d_i}{2\varepsilon_s}$$

$$\text{at } x = d_i,\ \phi = \phi_0 = \frac{2\pi qN_d d_i}{\varepsilon_s}$$

$$d_i = \left(\frac{\phi_0 \varepsilon_s}{2\pi qN_d}\right)^{1/2}$$

The thickness of the Scholtky barrier is given by

$$d_i = \frac{P_0}{qN_d} - \frac{4\pi\phi_i}{qN_d} \qquad (12)$$

where ϕ_i represents the surface charge localized at the levels of the ith surface. If the spontaneous polarization of the ferroelectric is completely screened by the charge of the surface levels, then $P_0 = 4\pi\phi_i$ and the barrier is not formed in accordance with Equation 12. The field in the surface equals

zero in this case. If, conversely, the charge of the surface levels can be neglected as compared to the spontaneous polarization, then

$$d_i \simeq \frac{P_0}{qN_d} \tag{13}$$

and, consequently, the thickness of the barrier is determined by the magnitude of the spontaneous polarization, and the concentration of donors (acceptors). According to equation 13, the higher the concentration of surface levels, the thinner the barrier. Using $P_0 = 1.1\ \mu C/cm$, $N_d \simeq 3 \times 10^{18} cm^{-3}$ obtained from equation

$$N_d = \frac{P_s^2}{2\varepsilon\varepsilon_0 \kappa t} \tag{14}$$

we get $d_i \simeq 230Å$, and the surface field $E_0 = 66$ kV/cm. Similar calculations for results on quartz substrates give

$N_d = \simeq 10^{20} cm^{-3}$, $d_i = 85Å$, and $E_0 = 215$ kV/cm.

In principle, however, the thickness of the barrier is not the same at the opposite ends of the domain, i.e., $d_+ \neq d_-$. This is due to the difference in volume concentrations of the donors and the acceptors, $N_d \neq N_a$, as well as the noncoincidence of the electrochemical potentials of the opposite surfaces. If we neglect the difference of electron affinity of the opposite ends, then the barrier height has the form

$$\phi_{0-} - \phi_{0+} \simeq 2 \frac{P_0}{qN_d} \tag{15}$$

Substituting the values in equation (15) we have $\phi_{0-} - \phi_{0+} \simeq .15$ eV for $BaTiO_3$ system and 0.25 for $BaTiO_3$ system.

Thus the surface levels in ferroelectric greatly influence its ferroelectric properties.

SUMMARY AND CONCLUSIONS

The current research reports the observations of reproducibly consistent ferroelectric $BaTiO_3$ (0.10 to 0.50 μm) films on silicon and quartz substrates. Ferroelectric behavior is regularly observed for $BaTiO_3$ films thicker than 0.1 μm that are rf sputter deposited at 5 Å/min in 15-22 μm Hg, 5% O_2/95% Ar mixtures onto silicon substrates at temperatures above 500°C. To obtain good quality ferroelectric films, the substrate temperature must be reduced during the last part of the deposition at a rate of 6 to 7°C/min to a final temperature of about 180-120°C. The x-ray diffraction and SEM analyses indicate that films with pervoskite type structures are obtained on silicon and quartz substrates. The measurements of P-E hysteresis loops, the dielectric constant peaks, and sense of the c-v curves (anticlockwise) have been used to confirm ferroelectricity of the rf sputtered $BaTiO_3$ films. A persistent problem with all the Mfs devices fabricated was that the value of the spontaneous polarization was low indicating some kind of hindrance in the polarization reversal mechanism. Between the silicon and the sputtered films an intermediate layer with a high concentration of defects is present. Therefore, in an effort to understand the quality of the sputtered films and the film/substrate interface, a detailed layer-by-layer analysis using the Scanning Auger microscope was carried out. Three kinds of layers were observed: an external surface layer consisting of carbon and an excess of barium up to

several tens of angstroms (50 - 80 Å) thick; a main layer with stable composition, but whose concentration depends on the evaporation condition; and an intermediate film-substrate layer consisting of reduced form of $TiO_{2-x}(x < 2)$. The thickness of the intermediate layer varied between 200-500 Å. It is these, the surface and the intermediate layers together with the defects in the main layer, that suppress the spontaneous polarization and give rise to a high value of coercive field. In contrast, the films formed on quartz substrates under identical conditions gave values for spontaneous polarization very close to the bulk value. These results again indicate that a severe interaction between the silicon and the $BaTiO_3$ sputtered films occurs.

This work also reports the first observation of the high photovoltaic (24×10^3 v/cm) effect in thin films of $BaTiO_3$ produced by rf sputtering. The results on open circuit and short circuit measurements illustrate the role of the photovoltaic field, photovoltaic currents, the photoconductance in photoferroelectric domain switching, and in general, provide an important basis for the better understanding of the observed phenomena. The present results further demonstrate that though the existence of anomalously large open circuit photovoltage in ceramics and single crystals is a well documented fact, theoretical explanations for this behavior need much work, especially from the thin film physics point of view.

If there is to be any hope of using the anomalously high voltage in device applications, it will be necessary first to carry out a detailed study on the characterization of the films. As observed here, severe interaction between silicon and $BaTiO_3$ is observed. This problem can apparently be solved by growing a pacification layer on the silicon substrate. Additional work is necessary to optimize the parameters of the pacification layer to minimize the interaction problem of the complicating effects of

tunneling while not affecting the ferroelectric properties of the crystalline $BaTiO_3$. However, furt her experimentation in this area would have required an effort beyond the support level provided.

In any future work, far greater attention should be paid to the physics of the photovoltaic mechanism in the physics of thin films. It seems very likely that the photovoltaic effect in $BaTiO_3$ thin films is a composite of the bulk effect found in ceramics and single crystals plus the effects associated with the asymmetric semiconductor-ferroelectric boundaries, due to the presence of spontaneous polarization; these might behave somewhat as an additive series connections of scholtky-like photodiodes.

REFERENCES

1. Brody, P. S. and F. Crowne, J. Electron Mater. 4, 955 (1975).

2. Park, J. K. and W. W. Grannemann, Ferroelectrics, 10, 217 (1976).

3. Panitz, J. K. G. and C. C. Hu, J. Va. Sci. Technol., 16, 315 (1979).

4. Jona, F. and Shirane, G., Ferroelectric crystals, Pergamon Press, MacMillan Company, New York (1962).

5. Tomaspolskii, Yu Ja and M. A. Sevostianov, Ferroelectrics, 13, 415 (1976).

6. Mehta, R. R., B. D. Silverman, and J. T. Jacobs, J. Appl. Phys., 44, 8 (1973), 2379.

7. Ivanchik, I. J., Soviet Physics, Solid State, 3, 2705 (1962).

8. Glass, A. M., D. Von der Linde, and T. J. Negran, J. Electron. Mater., 4, 915 (1975).

9. Salama, C. A. T. and E. Siciunas, J. Vac. Sci. Technol., 9, 91 (1971).

10. Harrison, W.A., J. Vac. Sci. Technol, 14, 883 (1977).

11. Swanson, H. E. and Fuyat, NBS Circular No. 539, 3 (1953).

12. Castellano, R. N. and L. G. Feinstein, J. Appl. Phys., 50, 4406 (1979).

13. Okazaki, K. and K. Nagata, J. Am. Ceram. Soc., 56, 82 (1973).

14. Sze, S. M., Physics of semiconductor devices (New York): Wiley, 1969) p. 425.

15. Land, C. E. and P. S. Percy, Ferroelectrics, 27 131 (1980).

16. Holloway, A. P. H. and H. J. Stein, J. Electrochemical Soc, 123, 723 (1976).

17. Davis, L. E., et al., Handbook of Auger Electron Spectroscopy 2nd Edition (Physical Electronics Industries, Inc., Eden Prairie, Minnesota) 1976.

18. Tomashpol'skii, Yu. Ya., E. N. Lubnin, and M. A. Sevost'yanov, Sov. Phys. Crystallogr., 22, 330 91977).

19. Treibwasser, S., Phys. Rev., 11, 100 91960).

20. Selyuk, V. B., 12 v. Adak. Nauk SSSR, Ser. Fiz, 35 1798 (1971).